Colored Gaussian Multiple Descriptions: Spectral-Domain Characterization and Time-Domain Design

Jan Østergaard, *Member, IEEE,* Yuval Kochman, *Member, IEEE,* and Ram Zamir, *Fellow, IEEE*

Abstract

It is well known that Shannon's rate-distortion function (RDF) in the colored quadratic Gaussian (QG) case, can be parametrized via a single Lagrangian variable (the "water level" in the reverse water filling solution). In this work, we show that the symmetric colored QG multiple-description (MD) RDF in the case of two descriptions, can be parametrized via two Lagrangian variables. To establish this result, we use two key ideas. First, we propose a new representation for the MD test channel, and show that the minimum mutual information rate across this channel coincide with the QG MD RDF. Second, we use variational calculus to obtain a spectral domain representation of the test channel's optimal side and central distortion spectra given the source spectral density and the side and central distortion constraints. The distortion spectra are specified via two Lagrangian parameters, which control the trade-off between the side distortion, the central distortion, and the coding rate. We also show that the symmetric colored QG MD RDF can be achieved by noise-shaped predictive coding, dithered quantization, and memoryless entropy coding. In particular, we show that the proposed MD test channel can be materialized by embedding two source prediction loops, one for each description, within a common noise shaping loop whose parameters are explicitly found from the spectral-domain characterization. The source prediction loops exploit the source memory, and thus reduce the coding rate. The noise-shaping loop, controls the trade-off between the side and the central distortions by shaping the quantization noise.

This work was presented in part at the IEEE Data Compression Conference, Snowbird, Utah, 2008.

J. Østergaard (janoe@ieee.org) is with the Department of Electronic Systems, Aalborg University, Aalborg, Denmark. The work of J. Østergaard is supported by the Danish Research Council for Technology and Production Sciences, grant no. 274-07-0383.

Y. Kochman (yuvalko@mit.edu) is with the Department of Electrical Engineering and Computer Science, Massachusetts Institute of Technology, Cambridge, MA 02139, USA.

R. Zamir (zamir@eng.tau.ac.il) is with the Department of Electrical Engineering-Systems, Tel Aviv University, Tel Aviv, Israel.

Index Terms

Multiple-description coding, rate-distortion theory, predictive coding, noise shaping, delta-sigma quantization, optimization, calculus of variations.

I. INTRODUCTION

The traditional multiple-description (MD) problem [1] considers a source X which is encoded into two descriptions Y_1 and Y_2, using rates R_1 and R_2, respectively. Given either one of these descriptions, the decoder produces a reconstruction $\hat{X}_1$ or $\hat{X}_2$ resulting in a distortion D_1 or D_2, respectively. If both descriptions are available, the reconstruction is $\hat{X}_C$ yielding a distortion D_C. The achievable MD rate region $\mathcal{R}$, denotes the convex hull of the set of rate pairs $\{(R_1, R_2)\}$ that allow descriptions $\{(Y_1, Y_2)\}$, which simultaneously yield individual distortions no greater than D_1 and D_2, and a joint distortion no greater than D_C. We are interested in the *symmetric* situation where the two side description rates are equal (balanced), $R = R_1 = R_2$, and the side distortions are also equal, $D_S = D_1 = D_2$. In this case, the MD rate-distortion function (RDF) is defined as the minimum achievable rate R that guarantees a distortion pair no greater than (D_S, D_C).

The MD quadratic RDF for memoryless Gaussian sources was found by Ozarow [1]. An achievable rate region for the case of stationary Gaussian sources was recently characterized by Chen et al. [2]. In particular, it was shown in [2] that the achievable rate region forms a closed and convex set and that the minimal description rates can be found by extremizing over all distortion spectra satisfying the individual side and central distortion constraints. No explicit solution to the optimal distortion spectra was found. However, some intuition towards a spectral domain characterization was provided. Specifically, it was shown that the optimal rates for stationary Gaussian sources can be expressed as the sum of rates of parallel channels, each one representing a frequency band. Each of the channels must be tuned to a minimum Ozarow MD rate for some frequency dependent distortion level. In some sense, this can be seen as a reverse "water-filling" approach where instead of having a flat water level as in the conventional single-description case, the water level is frequency dependent. The authors also pointed out that obtaining an explicit spectral domain solution from their results is technically non-trivial. Instead it was argued that the optimal rates can be found through numerical optimization by approximating the source

spectral density by piece-wise constant functions. However, in general, for arbitrarily shaped sources, this becomes an infinite-dimensional optimization problem.

In this paper, we present a parametrization of the symmetric colored QG MD RDF. While Shannon's RDF in the single description (SD) case can be parametrized by a single Lagrangian variable [6] (usually referred to as a "water level"), we show here that the symmetric colored QG MD RDF can be parametrized via two Lagrangian variables.[1] To establish this result, we use two key ideas. First, we propose a new representation for the MD test channel (see e.g., Fig. 11), and show that the minimum mutual information rate across this channel coincides with the QG MD RDF. Moreover, the mutual information rate is shown to be equal to the scalar mutual information over an AWGN channel, and the test channel can therefore be realized with white Gaussian quantization (e.g., high dimensional lattice quantization). Second, instead of taking the conventional approach of diagonalizing the colored Gaussian source and thereby obtain an infinite number of independent sources (which might result in an infinite-dimensional optimization problem) we show that it is possible (and feasible) to directly optimize over the continuum of the test channels' side and central distortion spectral densities through the use of calculus of variations [7]. The resulting distortion spectra are then specified via two Lagrangian parameters, which control the trade-off between the side distortion, the central distortion, and the coding rate. Thus, we avoid extremizing over all *functions* representing admissible distortion spectra subject to the two distortion constraints. Instead, our results reveal that this otherwise intractable infinite-dimensional optimization problem, can be cast as a two-dimensional optimization problem over two non-negative Lagrangian parameters subject to the same distortion constraints.

In [3], it was shown that Ozarow's white Gaussian MD RDF can be achieved by dithered Delta-Sigma quantization (DSQ) and memoryless entropy coding. Furthermore, by exploiting the fact that Ozarow's test channel becomes asymptotically optimal for stationary sources in the high-rate regime [4], it was shown in [3] that, at high resolution, the stationary MD RDF is achievable by DSQ and *joint* entropy coding. In [2] it is demonstrated how one can achieve any point on the boundary of the colored Gaussian achievable rate region $\mathcal{R}$ by a *frequency-domain* scheme, where the source is divided into sub-bands, and in each sub-band the "quantization-splitting" scheme for white Gaussian sources presented in [5] is applied.

[1] In our case, however, the two parameters cannot generally be interpreted as "water levels".

In this paper, we propose a *time-domain* approach: We show that the symmetric colored QG MD RDF can be achieved by noise-shaped predictive coding and *memoryless* dithered quantization (in the limit of high dimensional quantization) at all resolutions and all side-to-central distortion ratios. We establish this result by forming a nested prediction / noise-shaping structure containing a dithered DSQ scheme similar to [3] in the outer loop and a predictive coder per each description in the inner loop, see for example Fig. 12. Each of the predictive coders has the structure of the differential pulse-code modulation (DPCM) scheme, shown to be optimal in the SD setting in [8].[2] The role of the DSQ loop is to shape the quantization noise so that a desired trade-off between the side distortions and the central distortion is achieved. It was shown in [3] that the central distortion is given by the power of the noise that falls within the in-band spectrum (i.e. the part of the frequency spectrum which overlaps the source spectrum) whereas the side distortion is given by the power of the complete noise spectrum, i.e. the in-band and the out-of-band noise spectrum. It was furthermore shown that any ratio of side-to-central distortion can be obtained by proper shaping of the quantization noise. We establish a similar result here. In particular, the predictive coders take care of the source memory and thereby minimize the coding rate and make sure that memoryless entropy coding is optimal. Moreover, the DSQ loop performs the noise shaping, which is required in order to achieve any desired pair of distortions (D_S, D_C).

This paper is organized as follows. In section II, we provide the preliminaries. Then, in Section III, we propose a test channel, which provides a new interpretation of the QG MD RDF. We present the spectral-domain characterization of the optimal distortion spectra in Section IV. With the test channel in mind, we present, in Section V, an SD time-domain scheme which encodes a source subject to a distortion mask. Then, in Section VI, we extend the SD time-domain scheme of Section V to the MD case. Conclusions are in Section VII. Longer proofs are deferred to Appendices A–C.

[2]The idea of exploiting prediction in MD coding has previously been proposed by other authors, see for example the following related works [9]–[12]. All these works faced the basic problem: Since DPCM uses prediction from the reconstruction rather than from the source itself, and this prediction should be reproduced at the decoder, it is not clear which of the possible reconstructions should be used for prediction. The present work solves this problem.

II. PRELIMINARIES

Let $X = \{X[n]\}_{n=0}^{\infty}$ be a discrete-time stationary Gaussian process with power spectral density $S_X = \{S_X(e^{j\omega})\}_{\omega=-\pi}^{\pi}$. We assume that the spectrum S_X obeys the Paley-Wiener conditions [13], such that it has a positive entropy-power $0 < P_e(S_X) < \infty$, where the entropy power of a spectrum S_X is defined as:[3]

$$P_e(S_X) \triangleq \exp\left(\frac{1}{2\pi}\int_{-\pi}^{\pi} \log\left(S_X(e^{j\omega})\right) d\omega\right) \tag{1}$$

and where here and onwards all logarithms are taken to the natural base. Using this notation, a spectrum has a spectral decomposition:

$$S_X(e^{j\omega}) = \left.\frac{P_e(S_X)}{(1+A(z))(1+A^*\left(\frac{1}{z^*}\right))}\right|_{z=e^{j\omega}}, \tag{2}$$

where

$$A(z) = \sum_{i=1}^{\infty} a_i z^{-i}, \tag{3}$$

is the *optimal predictor* associated with the spectrum S_X.

In this work, we are interested in the symmetric case, where $R_1 = R_2 \triangleq R$ and $D_1 = D_2 \triangleq D_S$. The two descriptions $Y_1 = \{Y_1[n]\}$ and $Y_2 = \{Y_2[n]\}$, which are output by the encoder, are used individually by the decoder to produce $\hat{X}_1 = \{\hat{X}_1[n]\}$ and $\hat{X}_2 = \{\hat{X}_2[n]\}$, respectively. If both descriptions are available, the decoder produces the joint reconstruction $\hat{X}_C = \{\hat{X}_C[n]\}$. We will use the time-averaged mean squared error (MSE) as fidelity criterion. In particular, the corresponding MSE distortions are $D_S \triangleq \mathbb{E}[\bar{d}(X, \hat{X}_1)] = \mathbb{E}[\bar{d}(X, \hat{X}_2)]$, where $\bar{d}(\cdot,\cdot)$ is the time-averaged squared error, i.e.,

$$D_S = \lim_{k\to\infty} \frac{1}{k}\sum_{n=0}^{k-1} \mathbb{E}[(X[n] - \hat{X}_i[n])^2], \quad i = 1, 2, \tag{4}$$

and $D_C \triangleq \mathbb{E}[\bar{d}(X, \hat{X}_C)]$.

We will be using entropy-constrained dithered (lattice) quantizers (ECDQs) for which it is known that the additive noise model is exact at all resolutions [14]. We will furthermore assume

[3]For arbitrary distributed sources with finite differential entropy $h(X)$, $P_e(S_X) \triangleq \frac{1}{2\pi e} e^{2h(X)}$. For stationary Gaussian sources, $h(X) = \frac{1}{2}\log(2\pi e) + \frac{1}{4\pi}\int \log(S_X(e^{j\omega}))d\omega$ from which (1) follows.

the existence of a large number K of identical and mutually independent sources (or e.g. a single source which is divided into K long blocks and jointly encoded as K parallel sources, see [8] for details). These sources are treated independently, except for the actual ECDQ which processes them jointly. Thus we will only present the scheme for one source, but the quantization noise has the properties of a high-dimensional ECDQ (cf. [8]). We provide an asymptotic analysis in the limit $K \to \infty$. In this asymptotic case, the quantization noise becomes approximately Gaussian distributed (in a divergence sense) [15]. Thus, for analysis purposes, we can replace the quantizer with a white additive noise model where the noise is approximately Gaussian distributed.

We will also assume that the proposed system has been operating for a long time, so that possible short-time temporal transient effects can be ignored. Thus, we consider the system in steady state where it is time invariant and have well defined variances and power spectral densities.

A. Additional Notation

For x real or complex, $\sqrt[n]{x}$ has n roots. For $n = 2$ and $0 \leq x \in \mathbb{R}$ we define $\sqrt{x} \triangleq |\sqrt{x}|$, i.e., it is always non-negative. For $0 > x \in \mathbb{R}$ we define $\sqrt{x} \triangleq i|\sqrt{|x|}|$, i.e., we take the principal complex root. For $n = 3$ and $x \in \mathbb{R}$ we let $\sqrt[3]{x} \triangleq sign(x)|\sqrt[3]{|x|}|$ denote the unique real cubic root of x, e.g., $\sqrt[3]{-8} = -2$. If $x \in \mathbb{C}$ and $imag(x) \neq 0$, we let $\sqrt[3]{x}$ denote the principal complex root, i.e., it has a positive imaginary part. We use the notation ξ_i^{Ξ} to indicate the ith root of the function Ξ. If φ is a function of ζ, we use the notation $\varphi|_{\zeta=\lambda}$ to indicate that the function φ is evaluated at the point $\zeta = \lambda$.

III. The Quadratic Gaussian Symmetric MD Rate Revisited

In this section we re-state known results about the QG MD achievable rate in the symmetric case, in order to gain some insight and prepare the ground for what follows. In the high resolution limit, these results also hold for general sources with finite differential entropy rate [16].

For a white Gaussian source of variance σ_X^2, the minimum achievable symmetric side-descriptions rate was given by Ozarow [1]:

$$R_{white}(\sigma_X^2, D_C, D_S) \triangleq \frac{1}{4}\log\left(\frac{\sigma_X^2(\sigma_X^2 - D_C)^2}{4D_C(D_S - D_C)(\sigma_X^2 - D_S)}\right) \tag{5}$$

as long as $\frac{1}{D_C} \geq \frac{1}{D_{C,max}} = \frac{2}{D_S} - \frac{1}{\sigma_X^2}$. Under high-resolution conditions, i.e. $D_S \ll \sigma_X^2$, the above rate becomes:

$$R_{white,HR} = \frac{1}{2}\log\left(\frac{\sigma_X^2}{2\sqrt{D_C(D_S - D_C)}}\right) \tag{6}$$

as long as $D_C \leq D_{C,max,HR} \triangleq \frac{D_S}{2}$.

If the central decoder was to linearly combine two side descriptions of mutually independent distortions of variances D_S, it would achieve exactly the distortion $D_{C,max}$. This motivates the model of *negatively correlated* side distortions (see [4]). In the high resolution limit, the relation between the side and central distortions can be explained by the side distortions having a correlation matrix:

$$\Phi = D_S \begin{bmatrix} 1 & \rho \\ \rho & 1 \end{bmatrix}, \tag{7}$$

where $\rho = -\frac{D_S - 2D_C}{D_S} \leq 0$. With this notation, (6) becomes:

$$R_{white,HR} = \frac{1}{2}\log\left(\frac{\sigma_X^2}{\sqrt{|\Phi|}}\right) = \frac{1}{2}\log\left(\frac{\sigma_X^2}{D_S}\right) + \frac{1}{2}\log\left(\frac{1}{\sqrt{1-\rho^2}}\right) \triangleq \frac{1}{2}\log\left(\frac{\sigma_X^2}{D_S}\right) + \frac{1}{2}\delta_{HR}, \tag{8}$$

where δ_{HR} is the high-resolution excess rate [16]. Still in the high-resolution case, we take another step: Without loss of generality, we can represent the correlated noises as the sum of two mutually independent noises, one is added to both branches while the other is added to one branch and subtracted from the other, as depicted in Fig. 1. Note that the averaging eliminates

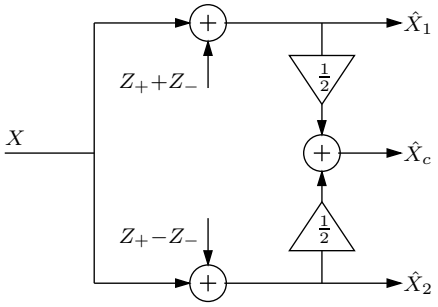

Fig. 1. A differential form of Ozarow's double-branch test channel for high resolution coding.

Z_- from the central description. If we denote the variances of the noises Z_+ and Z_- as Θ_+ and

Θ_-, respectively, then we can re-write (7) as:

$$\Phi = \begin{bmatrix} \Theta_+ + \Theta_- & \Theta_+ - \Theta_- \\ \Theta_+ - \Theta_- & \Theta_+ + \Theta_- \end{bmatrix}, \tag{9}$$

where the negative correlation $\rho < 0$ implies that $\Theta_- \geq \Theta_+$. In terms of these variances, we can define a spectrum:

$$\tilde{\Theta}(e^{j\omega}) \triangleq \begin{cases} 2\Theta_+, & |\omega| < \frac{\pi}{2}, \\ 2\Theta_-, & \frac{\pi}{2} \leq |\omega| < \pi. \end{cases} \tag{10}$$

With the above definitions, we have that the entropy-power (1) of $\tilde{\Theta}(e^{j\omega})$ is given by:

$$P_e(\tilde{\Theta}) = \sqrt{|\Phi|} = 2\sqrt{\Theta_+\Theta_-}$$

and consequently the MD rate is:

$$R = \frac{1}{2}\log\left(\frac{\sigma_X^2}{P_e(\tilde{\Theta})}\right). \tag{11}$$

The following proposition states this formally:

Proposition 1. *In the scheme of Fig. 1, let $\sigma_X^2/2 \geq \Theta_- \geq \Theta_+$. The distortions are given by:*

$$\begin{aligned} D_S &= \Theta_+ + \Theta_-, \\ D_C &= \Theta_+. \end{aligned} \tag{12}$$

In the high resolution limit, for these distortions, the minimum rate (6) *is given by* (11)*.*

Generalizing our view to all distortion levels, the equivalent channel is depicted in Fig. 2. A similar correlated-noises model to (7) can be obtained by expressing ρ in a rather complicated form. However, we can greatly simplify such an expression by proper use of pre- and post-factors as we show next. In a point-to-point scenario, it is convenient to make these factors equal [17], [14]. However, this is generally not possible in MD coding because the optimal post-factors (Wiener coefficients) are different for the side and central reconstructions. We choose the pre-factor to be equal to the *side* post-factor. While this choice seems arbitrary, it will prove useful

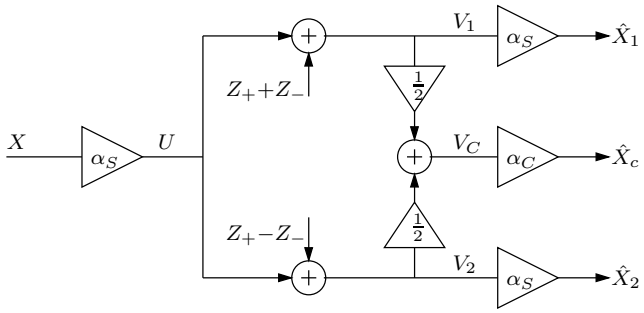

Fig. 2. Ozarow's test channel with pre and post factors.

when we turn to colored sources. Thus we have:

$$\begin{aligned} \alpha_S &\triangleq \sqrt{\frac{\sigma_X^2 - \Theta_+ - \Theta_-}{\sigma_X^2}}, \\ \alpha_C &\triangleq \frac{\alpha_S \sigma_X^2}{\alpha_S^2 \sigma_X^2 + \Theta_+} = \sqrt{\frac{\sigma_X^2(\sigma_X^2 - \Theta_+ - \Theta_-)}{(\sigma_X^2 - \Theta_-)^2}}. \end{aligned} \tag{13}$$

Proposition 2. *In the scheme of Fig. 2, let $\sigma_X^2/2 \geq \Theta_- \geq \Theta_+$. The distortions are given by:*

$$\begin{aligned} D_S &= \Theta_+ + \Theta_-, \\ D_C &= \frac{\sigma_X^2 \Theta_+}{\sigma_X^2 - \Theta_-}. \end{aligned} \tag{14}$$

For these distortions, the minimum achievable rate (5) *is given by* (11)*.*

Note that at high resolution conditions $\sigma_x^2 \gg \Theta_-$, so (14) reduces to (12).

Proof: Between U and $\{V_1, V_2, V_C\}$ we have exactly the high-resolution scheme of Proposition 1, i.e. we have $V_1 = U + Z_1$, $V_2 = U + Z_2$, $V_C = U + Z_C$, where $\{Z_1, Z_2, Z_C\}$ are independent of U, and where $\mathbb{E}[Z_1^2] = \mathbb{E}[Z_2^2] = \Theta_+ + \Theta_-$ and $\mathbb{E}[Z_C^2] = \Theta_+$. Since $\hat{X}_i = \alpha_S V_i$ and $\hat{X}_c = \alpha_C V_C$ it is, by use of (13), straightforward to show that $D_S = \mathbb{E}[(\hat{X}_i - X)^2]$ and $D_C = \mathbb{E}[(\hat{X}_C - X)^2]$ are given by (14). Now substitute these distortions in (5) to establish (11). ■

We now turn to general (colored) stationary Gaussian sources. In the high resolution limit, it was shown in [4] that the minimum rate is given by Ozarow's rate (5) with the source variance

σ_X^2 replaced by its entropy-power $P_e(S_X)$ (1). Recalling (11) we define:

$$R_{colored} \triangleq \frac{1}{2}\log\left(\frac{P_e(S_X)}{P_e(\tilde{\Theta})}\right), \tag{15}$$

where $\tilde{\Theta}$ is given by (10).

Proposition 3. *In the high resolution limit, for any $\Theta_- \geq \Theta_+$, the minimum achievable rate for the distortions.* (12) *is given by* (15)*.*

For general resolution, the achievable colored Gaussian MD rate region was characterized by Chen et al. [2]. In terms of our representation for the white case, we can re-write the result of [2] (for the symmetric case) in a parametric form. For given source spectrum S_X and noise spectra Θ_+ and Θ_-, we generalize (10) to the form:[4]

$$\tilde{\Theta}(e^{j\omega}) = \begin{cases} 2\Theta_+\left(e^{j2\omega}\right), & |\omega| < \frac{\pi}{2}, \\ 2\Theta_-\left(e^{j2\left(\omega-\frac{\pi}{2}\right)}\right), & \frac{\pi}{2} < \omega \leq \pi, \\ 2\Theta_-\left(e^{j2\left(\omega+\frac{\pi}{2}\right)}\right), & -\pi \leq \omega < -\frac{\pi}{2}. \end{cases} \tag{16}$$

With this, we define the distortion spectra (for $-\pi \leq \omega \leq \pi$):

$$D_S(e^{j\omega}) \triangleq \Theta_+(e^{j\omega}) + \Theta_-(e^{j\omega}) \tag{17}$$

$$D_C(e^{j\omega}) \triangleq \frac{S_X(e^{j\omega})\Theta_+(e^{j\omega})}{S_X(e^{j\omega}) - \Theta_-(e^{j\omega})}, \tag{18}$$

reflecting the use of pre- and post-filters. Then the result of [2] is equivalent in the symmetric case to the following Proposition and Corollary:

Proposition 4. *For any spectra*

$$S_X(e^{j\omega})/2 \geq \Theta_-(e^{j\omega}) \geq \Theta_+(e^{j\omega}) > 0, \ \forall\omega,$$

the minimum achievable side-description rate in symmetric MD coding of a Gaussian source with spectrum S_X with the side and central distortion spectra (17) and (18) is given by (15)*.*

[4]Notice that the lowpass and highpass spectra of $\tilde{\Theta}$ are formed by $\{\Theta_+(e^{j2\omega})\}$ and $\{\Theta_-(e^{j2\omega})\}$, which are compressed versions (by a factor of two) of the spectra $\Theta_+ = \{\Theta_+(e^{j\omega})\}_{\omega=-\pi}^{\pi}$ and $\Theta_- = \{\Theta_-(e^{j\omega})\}_{\omega=-\pi}^{\pi}$, respectively.

Proof: See Appendix A. ■

Corollary 1. *The optimum symmetric MD side-description rate is given by the minimization of* (15) *over all* Θ_+, Θ_- *such that the distortion spectra (17) and (18) satisfy:*

$$\frac{1}{2\pi}\int_{-\pi}^{\pi} D_S(e^{j\omega})\,d\omega \;\leq\; D_S \tag{19}$$

$$\frac{1}{2\pi}\int_{-\pi}^{\pi} D_C(e^{j\omega})\,d\omega \;\leq\; D_C. \tag{20}$$

In the high resolution limit, the optimal spectra Θ_+, Θ_- become flat, thus $\tilde{\Theta}$ becomes a two-step spectrum, as in [3]. In the next section, we provide an explicit solution for the optimal noise spectra Θ_+ and Θ_- and distortion spectra $\{D_S(e^{j\omega})\}$ and $\{D_C(e^{j\omega})\}$.

Remark 1. *If* X *does not satisfy the Paley-Wiener condition, then* (15)*, which is based on entropy powers, is not well defined. In this case, we may use the following: For any* $\epsilon > 0$*, let* $S_{X_\epsilon}(e^{j\omega}) = \max(S_X(e^{j\omega}), \epsilon), \forall\omega$*, and* $D_\epsilon = \frac{1}{2\pi}\int_{-\pi}^{\pi}\max(0, \epsilon - S_X(e^{j\omega}))d\omega$*. Then there exists some* $\epsilon > 0$ *such that Proposition 4 and Corollary 1 hold with* S_X*,* D_S*, and* D_C *replaced by* $S_{X_\epsilon}, D_S + D_\epsilon$*, and* $D_C + D_\epsilon$*, respectively.*

IV. Spectral Domain Characterization of the Two-Description RDF

In this section we provide a spectral domain characterization of the distortion spectra. We first recall from Corollary 1 that finding the RDF is equivalent to finding a pair of noise spectra $\Theta_+ = \{\Theta_+(e^{j\omega})\}_{\omega=-\pi}^{\pi}$ and $\Theta_- = \{\Theta_-(e^{j\omega})\}_{\omega=-\pi}^{\pi}$, which minimizes the description rate R subject to the two target distortion constraints D_S and D_C. This constrained minimization problem can also be formulated as a Lagrangian unconstrained problem, which then provides a two-parameter characterization of the RDF. Specifically, we consider the problem of minimizing the functional J where

$$J = R + \lambda_1 D_S + \lambda_2 D_C, \tag{21}$$

and where $R = \frac{1}{4\pi}\int_{-\pi}^{\pi}\log\left(\frac{S_X(e^{j\omega})}{2\sqrt{\Theta_+(e^{j\omega})\Theta_-(e^{j\omega})}}\right)d\omega$ and D_S and D_C are given by the inequality constraints (19) and (20), respectively. The scalar weights λ_1 and λ_2 are non-negative Lagrangian variables, which provide a trade-off between rate, side distortion, and central distortion. Intuitively, letting $\lambda_1 \approx 0, \lambda_2 \approx 0$, results in a rate close to zero since this is equivalent to solving a minimization problem without any constraints (except that of a non-zero rate). On the other

hand, letting $\lambda_1 \gg 1$ or $\lambda_2 \gg 1$ penalizes one of the distortions and corresponds to a high rate situation. In particular, if $\lambda_1 \gg \lambda_2$, then the side distortion is severely penalized and is therefore forced to be small. The central distortion is of less concern in this case. If $\lambda_2 \gg \lambda_1$, then the central distortion is minimized and the side distortion is of less concern. Finally, if both $\lambda_1, \lambda_2 \gg 1$, then both the side and central distortions are small.

At this point, we define

$$\Xi(e^{j\omega}) \triangleq q^2(e^{j\omega}) + p^3(e^{j\omega}), \tag{22}$$

which is the discriminant of a third-order polynomial, see (79) in Appendix B, and where

$$\begin{aligned} p(e^{j\omega}) = -\frac{1}{144\lambda_1^2}(&-8\lambda_1 S_X(e^{j\omega}) - 16\lambda_2 S_X(e^{j\omega}) + 16\lambda_1\lambda_2 S_X^2(e^{j\omega}) + 16\lambda_1^2 S_X^2(e^{j\omega}) \\ &+ 16 S_X^2(e^{j\omega})\lambda_2^2 + 1) \end{aligned} \tag{23}$$

and

$$\begin{aligned} q(e^{j\omega}) = -\frac{1}{1728\lambda_1^3}\Big(&96\lambda_1\lambda_2 S_X^2(e^{j\omega}) - 48\lambda_1^2 S_X^2(e^{j\omega}) - 64\lambda_2^3 S_X^3(e^{j\omega}) - 96\lambda_2^2 S_X^3(e^{j\omega})\lambda_1 \\ &+ 96\lambda_2^2 S_X^2(e^{j\omega}) + 96\lambda_2 S_X^3(e^{j\omega})\lambda_1^2 + 24\lambda_2 S_X(e^{j\omega}) + 64\lambda_1^3 S_X^3(e^{j\omega}) + 12\lambda_1 S_X(e^{j\omega}) - 1\Big). \end{aligned} \tag{24}$$

With this, we let $\phi(e^{j\omega})$ be given by:

$$\phi(e^{j\omega}) = \begin{cases} \arctan\left(\frac{\sqrt{-\Xi(e^{j\omega})}}{q(e^{j\omega})}\right), & q(e^{j\omega}) > 0, \\ \pi + \arctan\left(\frac{\sqrt{-\Xi(e^{j\omega})}}{q(e^{j\omega})}\right), & q(e^{j\omega}) < 0, \\ \pi/2, & q(e^{j\omega}) = 0. \end{cases} \tag{25}$$

We are now in a position to present the two-description RDF in a parametric form:

Theorem 1. *Let X be stationary Gaussian with spectral density S_X, and having finite positive differential entropy rate, i.e., $0 < \bar{h}(X) < \infty$. Then the symmetric two-description RDF, $R_X(D_S, D_C)$, of X at positive distortions $D_S > D_C > 0$ and under the MSE fidelity criterion is given by:*

$$R_X(D_S, D_C) = \frac{1}{4\pi}\int_{-\pi}^{\pi} \log\left(\frac{S_X(e^{j\omega})}{2\sqrt{\Theta_+(e^{j\omega})\Theta_-(e^{j\omega})}}\right) d\omega, \tag{26}$$

$$\Theta_-(e^{j\omega}) = \begin{cases} -\sqrt{|p(e^{j\omega})|}(\cos(\phi(e^{j\omega})/3) + \sqrt{3}\sin(\phi(e^{j\omega})/3)) + \frac{S_X(e^{j\omega})}{3\lambda_1}(2\lambda_1+\lambda_2) + \frac{1}{12\lambda_1}, \text{if } \Xi < 0, \\ \sqrt[3]{q(e^{j\omega}) + \sqrt{\Xi(e^{j\omega})}} - \sqrt[3]{q(e^{j\omega}) - \sqrt{\Xi(e^{j\omega})}} + \frac{S_X(e^{j\omega})}{3\lambda_1}(2\lambda_1+\lambda_2) + \frac{1}{12\lambda_1}, \text{if } \Xi(e^{j\omega}) \geq 0. \end{cases} \tag{28}$$

where the noise spectrum Θ_+ is given by

$$\Theta_+(e^{j\omega}) = \frac{S_X(e^{j\omega}) - \Theta_-(e^{j\omega})}{4S_X(e^{j\omega})(\lambda_1+\lambda_2) - 4\lambda_1\Theta_-(e^{j\omega})}, \quad -\pi \leq \omega \leq \pi, \tag{27}$$

and where Θ_-, for any $\lambda_1, \lambda_2 > 0$, is given by (28) (see top of page 13). Furthermore, the pair $(\lambda_1 > 0, \lambda_2 > 0)$ of Lagrangian parameters is chosen such that the distortion constraints are satisfied i.e.,

$$D_S \geq \frac{1}{2\pi}\int_{-\pi}^{\pi} \Theta_-(e^{j\omega}) + \frac{S_X(e^{j\omega}) - \Theta_-(e^{j\omega})}{4S_X(e^{j\omega})(\lambda_1+\lambda_2) - 4\lambda_1\Theta_-(e^{j\omega}) +} \, d\omega, \tag{29}$$

$$D_C \geq \frac{1}{2\pi}\int_{-\pi}^{\pi} \frac{S_X(e^{j\omega})}{4S_X(e^{j\omega})(\lambda_1+\lambda_2) - 4\lambda_1\Theta_-(e^{j\omega})} \, d\omega. \tag{30}$$

Proof: See Appendix B. ■

To elucidate the behavior of the noise spectra Θ_- and Θ_+ as a function of λ_1 and λ_2, we present the following results and examples.

Proposition 5 (High-Rate Cases)**.** *For any $\omega \in [-\pi; \pi]$,*

$$\lim_{\substack{\lambda_1,\lambda_2\to\infty \\ \lambda_1/\sqrt[3]{\lambda_2}\to 0}} \lambda_1\Theta_-(e^{j\omega}) = \frac{1}{4} \tag{31}$$

and

$$\lim_{\substack{\lambda_1,\lambda_2\to\infty \\ \lambda_1/\sqrt[3]{\lambda_2}\to 0}} (\lambda_1+\lambda_2)\Theta_+(e^{j\omega}) = \frac{1}{4}. \tag{32}$$

Proof: See Appendix C. ■

Remark 2. *The convergence requirement of $\lambda_1/\sqrt[3]{\lambda_2} \to 0$ in Proposition 5 is a technicality needed in the proof. As shown in Fig. 3, the limiting behavior of (31) and (32) can also be observed for small λ_2 and large λ_1. This shows that under high-resolution conditions, the optimum noise spectra are flat and approximately given by $\Theta_-(e^{j\omega}) \approx \frac{1}{4\lambda_1}$ and $\Theta_+(e^{j\omega}) \approx \frac{1}{4(\lambda_1+\lambda_2)}$.*

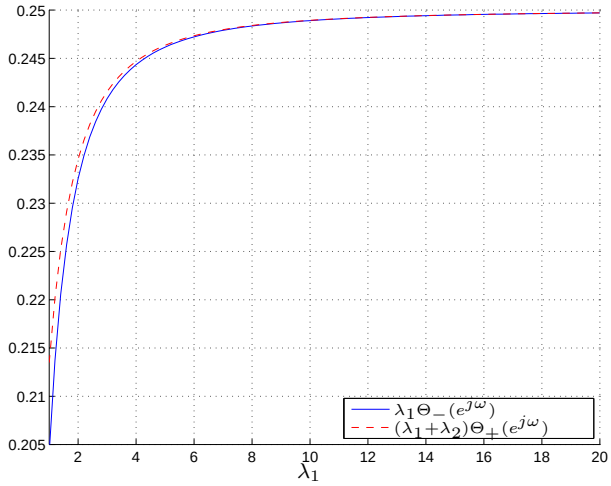

Fig. 3. High-rate convergence of $(\lambda_1+\lambda_2)\Theta_+(e^{j\omega})$ and $\lambda_1\Theta_-(e^{j\omega})$ as $\lambda_1 \to \infty$ when $S_X(e^{j\omega}) = 1, \lambda_2 = 2$ and any ω.

Example 1. *Let the source have a positive and monotonically decreasing spectrum given by*

$$S_X(e^{j\omega}) = \cos(\omega) + 1, \quad 0 \leq |\omega| < \pi, \tag{33}$$

and shown in Fig. 4. Moreover, let the distortion constraints be $D_C = 0.08$ *and* $D_S = 0.4$.

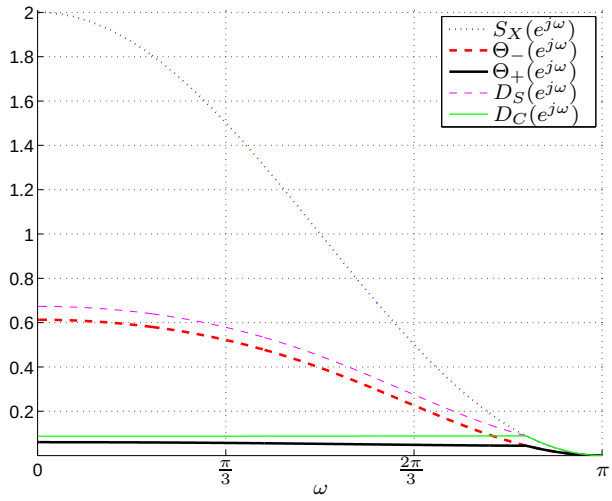

Fig. 4. Source S_X, noise Θ_+, Θ_-, and distortion $\{D_S(e^{j\omega})\}$, $\{D_S(e^{j\omega})\}$ spectra for $0 \leq |\omega| < \pi$.

Using the closed-form expressions for the noise spectra provided by Theorem 1, we have numerically performed a simple grid search over λ_1 *and* λ_2. *As* λ_1 *and* λ_2 *are varied, we*

compared the resulting side and central distortions given by (29) and (30), respectively, to the above mentioned distortion contraints D_S and D_C. The noise spectra that resulted in distortions closest to the constraints are shown in Fig 4. The spectra were obtained with $\lambda_1 = 0.2380$, and $\lambda_2 = 2.700$, which resulted in $D_C = 0.0801$ and $D_S = 0.4000$. Moreover, when using these spectra in (26) the obtained per description rate is $R = 0.7468$ bits/dim. In Fig. 4, we have also shown the resulting side and central distortion spectra using (17) and (18), respectively.

To better illustrate the trade-off between central and side distortions as a function of the source spectrum, we have shown the ratio $\log(\Theta_-(e^{j\omega})/\Theta_+(e^{j\omega}))$ as well as the ratio $\log(D_S(e^{j\omega})/D_C(e^{j\omega}))$ in Fig. 5. Also shown in Fig. 5, is the sum-rate $2R(e^{j\omega})$ allocated to each frequency band, where $R(e^{j\omega})$ denotes the per description rate spectral density, which is given by

$$R(e^{j\omega}) = \frac{1}{2}\log_2(S_X(e^{j\omega})/(2\sqrt{\Theta_+(e^{j\omega})\Theta_-(e^{j\omega})})). \tag{34}$$

It may be noticed that zero rate is allocated for the part of the source spectrum, which lies below a certain threshold (as is also the case in conventional SD reverse water-filling).

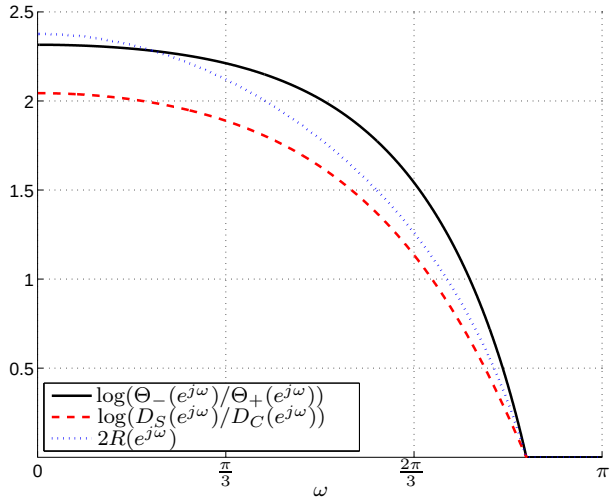

Fig. 5. Noise spectra ratio $\log(\Theta_-(e^{j\omega})/\Theta_+(e^{j\omega}))$, and distortion spectra ratio $\log(D_S(e^{j\omega})/D_S(e^{j\omega}))$ as a function of the source spectrum given by (33). Also shown is the sum-rate spectral density $2R(e^{j\omega})$ (in this latter case, the y-axis represents bits/dim. instead of distortion ratios).

Example 2. *For a given $\omega \in [-\pi;\pi]$ let $S_X(e^{j\omega}) = 2$ and let $\lambda_1 = 3$. Then the noise spectral density components $\Theta_-(e^{j\omega})$ and $\Theta_+(e^{j\omega})$ are shown in Fig. 6 (expressed in dB) as a function*

of λ_2 in the range $[0;10]$. For $\lambda_2 < 0.52$, the discriminant Ξ is positive whereas for $\lambda_2 > 0.52, \Xi$ is negative. We have indicated the switching point with circles in the figure. Notice that already at e.g., $\lambda_2 = 4$, the approximation $\frac{1}{4(\lambda_1+\lambda_2)}$ of (32), i.e., $-10\log_{10}(4(\lambda_1+\lambda_2)) = -14.47$ dB provides a good approximation of $\Theta_+(e^{j\omega})$. Also shown in Fig. 6, are $\Theta_-(e^{j\omega})$ and $\Theta_+(e^{j\omega})$ as a function of $\lambda_1 \in [0;10]$ for fixed $\lambda_2 = 3$ and $S_X(e^{j\omega}) = 2$. In this case, $\Xi < 0$ for all λ_1. Notice that at $\lambda_1 = 4$, the approximation $\frac{1}{4\lambda_1}$ of (31), i.e., $-10\log_{10}(4\lambda_1) = -12.04$ and (32), i.e., $-10\log_{10}(4(\lambda_1+\lambda_2)) = -14.47$, provide good approximations of $\Theta_-(e^{j\omega})$ and $\Theta_+(e^{j\omega})$, respectively. As $\lambda_1 \to 0$, $\Theta_-(e^{j\omega}) \to S_X(e^{j\omega})/2$, and since $\lambda_2 > 0$, the rate is used entirely for reducing the central distortion. However, as λ_1 increases, more rate is spend on decreasing $\Theta_-(e^{j\omega})$ with less emphasis on $\Theta_+(e^{j\omega})$.

The side and central distortions $D_S(e^{j\omega})$ and $D_C(e^{j\omega})$ for the above $\Theta_-(e^{j\omega})$ and $\Theta_+(e^{j\omega})$ and given ω are shown in Fig. 7. In Fig. 8, we have illustrated $\Theta_-(e^{j\omega}), \Theta_+(e^{j\omega}), D_S(e^{j\omega})$, and $D_C(e^{j\omega})$ as functions of $\lambda_1 = \lambda_2$, and the corresponding description rate spectral densities $R(e^{j\omega})$, given by (34), are shown in Fig. 9.

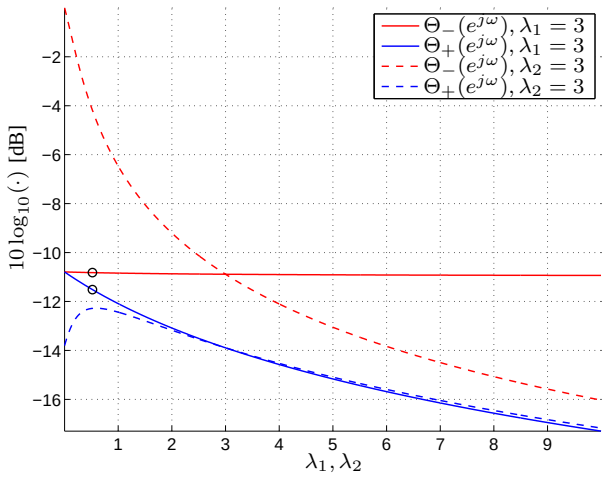

Fig. 6. $\Theta_-(e^{j\omega})$ and $\Theta_+(e^{j\omega})$ as functions of λ_1 and as functions of λ_2. The circles indicate when Ξ switches from being positive to become negative, which corresponds to the cases given by (28). A single frequency bin where $S_X(e^{j\omega}) = 2$ is considered.

V. Time-Domain Source Coding Subject to a Distortion Mask

We take a detour to a problem that is suggested by Proposition 4; coding of a source subject to a maximum distortion *mask* $D = \{D(e^{j\omega})\}_{\omega=-\pi}^{\pi}$, rather than subject to a total distortion

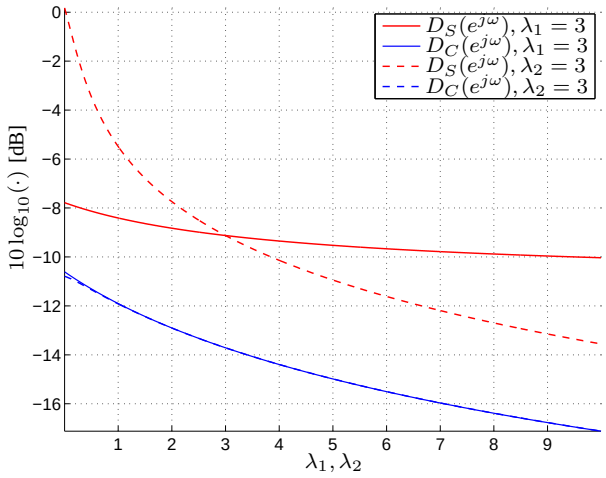

Fig. 7. $D_C(e^{j\omega})$ and $D_S(e^{j\omega})$ as functions of λ_1 and as functions of λ_2. A single frequency bin where $S_X(e^{j\omega}) = 2$ is considered.

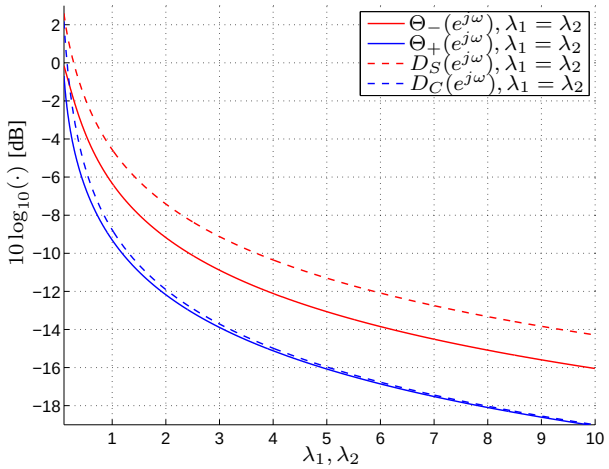

Fig. 8. $\Theta_-(e^{j\omega}), \Theta_+(e^{j\omega}), D_C(e^{j\omega})$, and $D_S(e^{j\omega})$ as functions of $\lambda_1 = \lambda_2$. A single frequency bin ω where $S_X(e^{j\omega}) = 2$ is considered.

constraint. This is an SD problem, but the solution will be extended to the MD problem in the following section. Without loss of generality[5], we assume that $D(e^{j\omega}) \leq S_X(e^{j\omega}), \forall\omega$. It is easy

[5]Otherwise, there is just wasted allowed distortion which does not serve to reduce the rate.

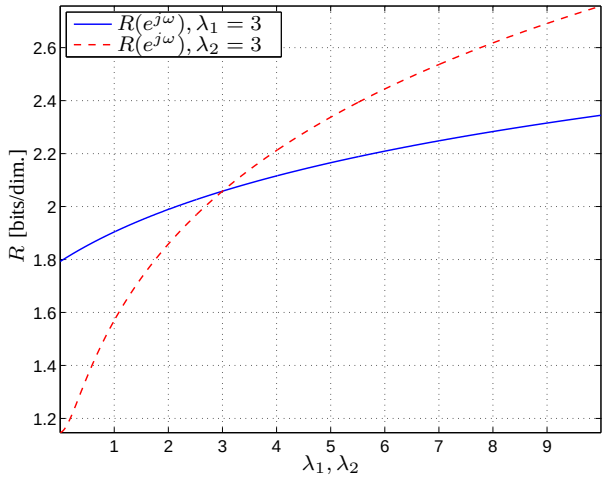

Fig. 9. $R(e^{j\omega})$ as a function of λ_1, as a function of λ_2, and as a function of $\lambda_1 = \lambda_2$. A single frequency bin where $S_X(e^{j\omega}) = 2$ is considered.

to verify, that the minimum rate for this problem is given by (recall (15)):

$$R\Big(S_X, D\Big) = \frac{1}{2}\log\left(\frac{P_e(S_X)}{P_e\Big(D\Big)}\right). \tag{35}$$

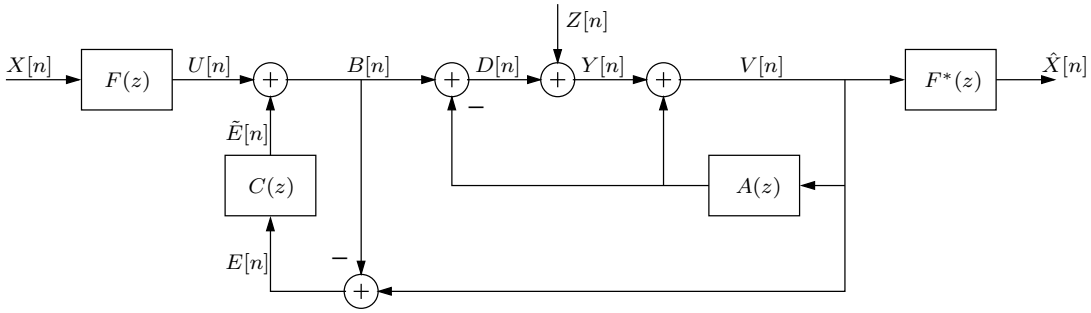

Fig. 10. A DSQ/DPCM equivalent channel for SD coding subject to a distortion mask.

Fig. 10 presents a *time-domain* scheme which achieves this rate. Motivated by the ratio of entropy powers (35), we strive to achieve the optimal rate by the combination of *source prediction* in order to present the quantizer with a prediction error of power $P_e(S_X)$, and *noise shaping*

in order to shape the white quantization noise of power $P_e(D)$ into the spectrum D.[6] These two tasks, we perform by a DPCM loop [8] and a noise-shaping loop [3], respectively. In this scheme, $Z[n]$ is AWGN of variance $P_e(D)$ and $A(z)$, which is given by (3), is the optimal predictor of the source spectrum S_X.[7] Moreover, $Q(z)$ given by

$$Q(z) = \sum_{i=1}^{\infty} q_i z^i, \tag{36}$$

is the optimal predictor for the equivalent distortion spectrum D, i.e., for $z = e^{j\omega}$,

$$D(e^{j\omega}) = P_e(D) \left| \frac{1}{1 + Q(e^{j\omega})} \right|^2 \tag{37}$$

$$= P_e(D) \left| 1 + C(e^{j\omega}) \right|^2, \tag{38}$$

from which it follows that the noise-shaping filter $C(e^{j\omega})$ is given by

$$C(e^{j\omega}) = -\frac{Q(e^{j\omega})}{1 + Q(e^{j\omega})}. \tag{39}$$

Note that $E[n]$, the input to the noise-shaping filter, is equal to $Z[n]$. The pre-filter $F(e^{j\omega})$ satisfies:

$$|F(e^{j\omega})|^2 = \frac{S_X(e^{j\omega}) - D(e^{j\omega})}{S_X(e^{j\omega})}. \tag{40}$$

Theorem 2. *The channel of Fig. 10 with the choices above, satisfies:*

$$S_{\hat{X}-X}(e^{j\omega}) = S_{V-U}(e^{j\omega}) = D(e^{j\omega}), \quad -\pi \le \omega \le \pi, \tag{41}$$

with the scalar *mutual information* $I(D[n]; Y[n]) = R\Big(S_X, D\Big)$ *of* (35)*.*

Proof: Since $E[n] = Z[n]$, we have that $V[n] = U[n] + Z[n] * (1 + c[n])$ so $V[n]$ and $U[n]$ are connected by an additive noise channel with noise spectrum D. From here, using the pre/post filter given by (40), the distortions follow immediately. Since the distortion spectra $\{S_{\hat{X}-X}(e^{j\omega})\}$ and $\{S_{V-U}(e^{j\omega})\}$ are equivalent and are furthermore equal to D, it also means that the mutual information rate $\bar{I}(\{U[n]\}; \{V[n]\}) = \bar{I}(\{X[n]\}; \{\hat{X}[n]\})$ equals the desired rate

[6] An alternative time-domain approach, is to accommodate for the distortion mask by changing the pre and post-filters. However, we choose the noise-shaping approach for the sake of extending this scheme to the MD setting.

[7] We assume that the optimal predictor $A(z)$ for the source spectrum exists. If not, then we may use the procedure outlined in Remark 1 in order to construct a predictor, which satisfies the assumption.

(35). We will now show that $\bar{I}(\{U[n]\};\{V[n]\}) = \bar{I}(\{B[n]\};\{V[n]\})$. To do so, we form the following sequence of equalities:

$$\bar{I}(\{U[n]\};\{V[n]\}) = \bar{h}(\{V_n\}) - \bar{h}(\{V_n\}|\{U_n\}) \tag{42}$$

$$= \bar{h}(\{V_n\}) - \bar{h}(\{U_n + (1+c[n]) * Z_n\}|\{U_n\}) \tag{43}$$

$$= \bar{h}(\{V_n\}) - \bar{h}(\{(1+c[n]) * Z_n\}) \tag{44}$$

$$= \bar{h}(\{V_n\}) - h(Z_n), \tag{45}$$

where the last equality follows since $1 + C(z)$ is monic and minimum phase. Similarly, using that $V_n = B_n + Z_n$, we can show that

$$\bar{I}(\{B[n]\};\{V[n]\}) = \bar{h}(\{V_n\}) - \bar{h}(\{V_n\}|\{B_n\}) \tag{46}$$

$$= \bar{h}(\{V_n\}) - \bar{h}(\{B_n + Z_n\}|\{B_n\}) \tag{47}$$

$$= \bar{h}(\{V_n\}) - \bar{h}(\{Z_n\}) \tag{48}$$

$$= \bar{h}(\{V_n\}) - h(Z_n), \tag{49}$$

which equals (45). At this point we notice that the channel from B to V contains a DPCM loop. Thus, we can apply [8, Theorem 1] to show that the mutual information rate $\bar{I}(\{B[n]\};\{V[n]\})$ across the channel $B \leftrightarrow V$ is equal to the scalar mutual information $I(D_n; D_n + Z_n)$ across the inner AWGN channel $D \leftrightarrow Y$. ■

Remark 3. *In the special case of a white distortion mask D, the constraint becomes (by the water-filling principle) equivalent to a regular quadratic distortion constraint. Indeed, the channel collapses in this case to the pre/post filtered DPCM channel of [8]. Much of the analysis there remains valid for this problem as well. In particular, we can construct an optimal coding scheme using this channel, substituting the AWGN for an ECDQ, and the scalar mutual information $I(D[n];Y[n])$ is also equal to the directed mutual information $I(D[n] \to Y[n])$.*

VI. Optimal Time-Domain Colored MD Coding

The similarity between the rates (15) and (35) is evident. We also note, that Theorem 2 deals with achieving the minimum rate subject to a distortion mask constraint, while Proposition 4 tells us that we must minimize the rate subject to *two* distortion mask constraints.

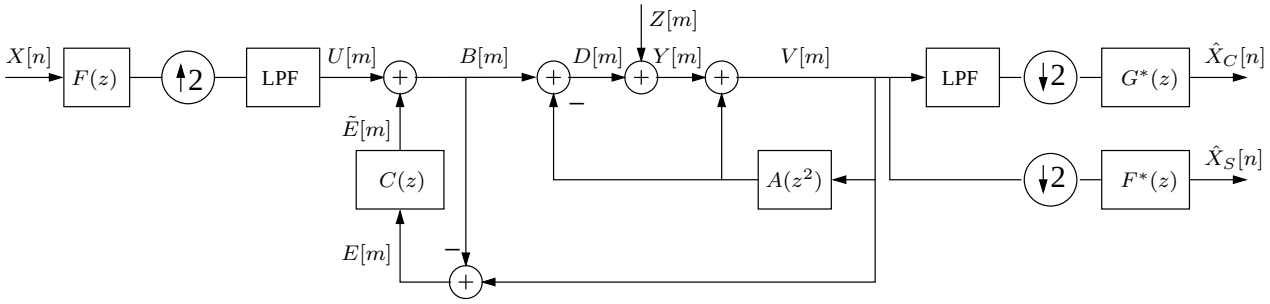

Fig. 11. A DSQ/DPCM equivalent channel for MD coding of a colored source.

Fig. 11 shows the adaptation of the distortion-mask equivalent channel to the MD problem.[8] Following [3], we combine upsampling by a factor of two with the noise-shaping loop, forming a DSQ loop. $Q(z)$ and $A(z)$ are the optimal predictors (2) of the spectra $\tilde{\Theta}$ and S_X, as before. Note that we apply an upsampled version of the source predictor, namely $A(z^2)$. Since the two side descriptions consist of the even and odd instances of $V[m]$, this is equivalent to applying the predictor $A(z)$ to each description in the original source rate. The DSQ loop, on the other hand, works in the upsampled rate and the noise-shaping filter $C(z)$ is given by (39). For a white source, $A(z) = 0$ and the channel reduces to the DSQ MD scheme of [3], while for optimal side distortion, $C(z) = 0$, and the channel reduces to an upsampled version of the DPCM equivalent channel of [8].

The filters $F(e^{j\omega})$ and $G(e^{j\omega})$ play the roles of pre/post filters and satisfy ($\forall\omega$):

$$\begin{aligned} |F(e^{j\omega})|^2 &= \frac{S_X(e^{j\omega}) - \Theta_+(e^{j\omega}) - \Theta_-(e^{j\omega})}{S_X(e^{j\omega})} \\ G(e^{j\omega}) &= \frac{S_X(e^{j\omega})}{S_X(e^{j\omega}) - \Theta_-(e^{j\omega})} F(e^{j\omega}). \end{aligned} \tag{50}$$

Theorem 3. *The channel of Fig. 11 with the choices above, satisfies:*

$$\begin{aligned} S_{\hat{X}_C - X}(e^{j\omega}) &= D_C(e^{j\omega}), \quad -\pi \le \omega \le \pi, \\ S_{\hat{X}_S - X}(e^{j\omega}) &= D_S(e^{j\omega}), \quad -\pi \le \omega \le \pi, \end{aligned} \tag{51}$$

[8]We use the index n for sequences which are "running" at the source rate, and the index m when referring to the upsampled rate.

where the distortion spectra were defined in (17) and (18), while the scalar *mutual information* $I(D[m];Y[m])$ *equals the rate* $R_{colored}$ *of* (15)*.*

Proof: The derivations of the distortion spectra $\{D_C(e^{j\omega})\}$ and $\{D_S(e^{j\omega})\}$ proceed similarly to the first part of the proof of Proposition 4 in Appendix A. That the mutual information rate $\bar{I}(\{B[m]\};\{V[m]\})$ equals (15) follows from the second part of the proof of Proposition 4. Finally, from the proof of Theorem 2, it follows that the mutual information rate $\bar{I}(\{U[m]\};\{V[m]\}) = \bar{I}(\{B[m]\};\{V[m]\}) = I(D[m];Y[m])$, i.e., it is equal to the scalar mutual information. ■

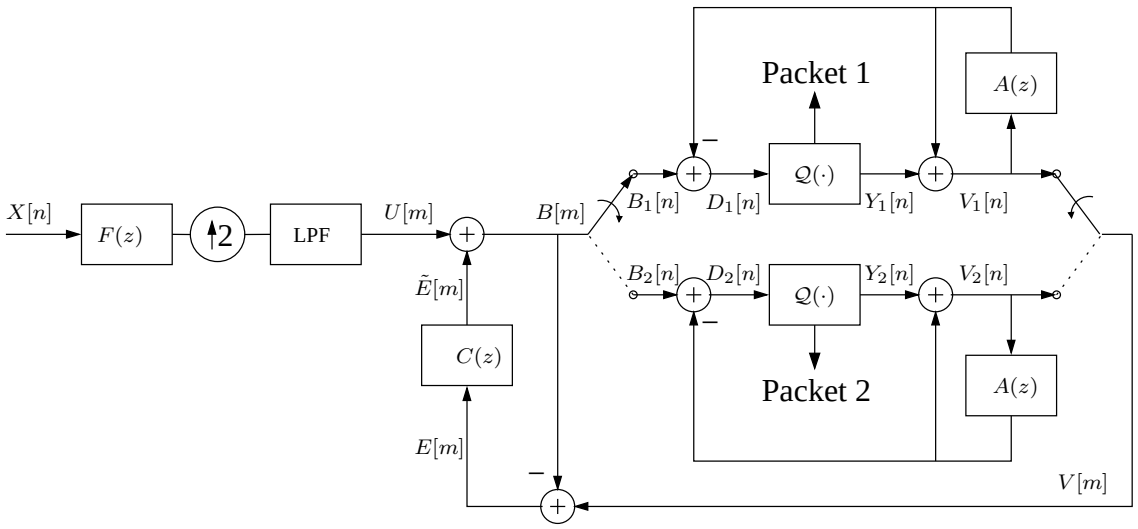

Fig. 12. Nested DSQ/DPCM MD encoder.

The encoder and decoder which materialize this equivalent channel are presented in Fig. 12 and Fig. 13, respectively. All of the switches in the encoder and the decoder are synchronized.[9] The up sampling operation followed by lowpass filtering introduces a half-sample delay on the odd samples. This delay is corrected at the decoder by the delay operator z^{-1} combined with the pair of up and downsamplers, see Fig. 13. The outputs of the quantizer blocks $\mathcal{Q}(\cdot)$ are the reconstructed values $Y_1[k]$ and $Y_2[k]$. Moreover, at each time k, the codeword of quantizer 1 (quantizer 2) is entropy-coded (conditioned upon the dither signal) and put into packet 1 (packet

[9]It is to be understood that the switches change their positions with the upsampled rate (m). Thus, in the encoder shown in Fig. 12, the even samples $B_1[n]$ of $B[m]$ will go on the upper branch and the odd samples $B_2[n]$ will go on the lower branch.

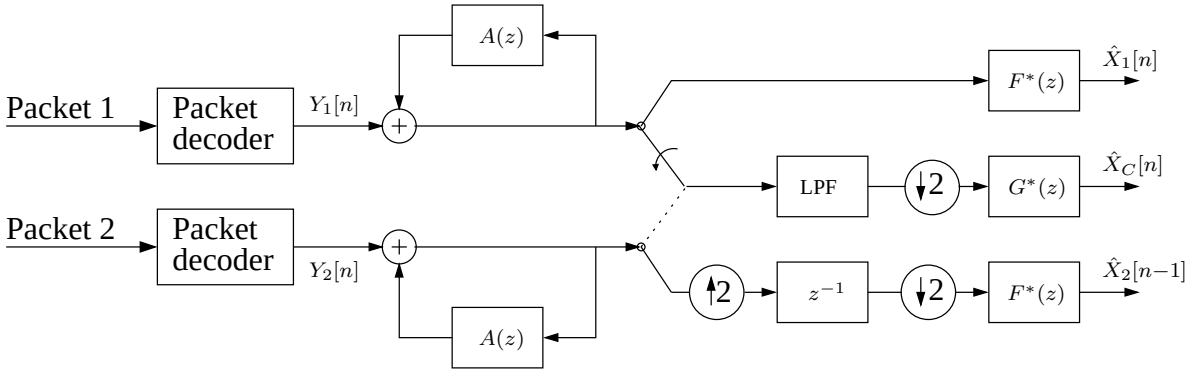

Fig. 13. DSQ/DPCM MD decoder.

2). The packet encoding operation is reversed at the decoder in order to obtain $Y_1[k]$ or $Y_2[k]$. If each quantizer block is taken to be a high-dimensional ECDQ with the required rate, and the two quantizer dither sequences are mutually independent, then these quantizers are equivalent to the additive noise $Z[m]$ of the equivalent channel. Consequently, the two descriptions $Y_1[n]$ and $Y_2[n]$ are equivalent to the odd and even samples, respectively, of $Y[m]$ in the equivalent channel, and finally the whole scheme from the source to the central and side reconstructions is equivalent to the channel from $X[n]$ to $\hat{X}_C[n]$ and $\hat{X}_S[n]$, respectively.

Since we see that this scheme achieves the optimal rate for any choice of spectra, it will become globally optimal when its parameters are chosen according to the minimizing spectra of Theorem 1. Thus, the encoder/decoder pair of Figs. 12 and 13 is able to achieve the complete symmetric quadratic MD RDF for stationary Gaussian sources at all resolutions and for any desired side-to-central distortion ratio.

Remark 4. *In the scheme shown in Fig. 12, the two prediction loops are embedded within a common noise shaping loop. Alternatively, one may alter the nesting order and let the common noise shaping loop be embedded within the two prediction loops. At high-resolution conditions, there is no loss of performance by switching the nesting order. However, at general resolution, the latter approach is suboptimal. The reason is, that for white quantization noise, the DPCM loop also shows to the outside a total white noise (by the basic DPCM equality [18]), while the DSQ loop shapes the noise. Since the DPCM loop assumes white noise for optimality [8], it cannot be built around the shaped DSQ noise.*

VII. Conclusions and Discussion

A parametric formulation of the two-description symmetric RDF for stationary colored Gaussian sources and MSE was presented. This result was established by providing a spectral domain characterization of the optimum side and central distortion spectra. For white Gaussian sources, the optimum distortion spectral density is a two step function. For colored sources, the optimum distortion spectral density is generally not piece-wise flat but depends upon the source spectral density and the desired resolution (i.e., the desired central and side distortion levels). It was furthermore shown that the symmetric MD RDF could be be achieved by a time-domain approach based on prediction and noise-shaping. The time domain implementation demonstrated that it was possible to separate the mechanism responsible for exploiting the source memory (DPCM) from the mechanism controling the MD coding parameters (noise shaping).

Appendix A
Proof of Proposition 4

We will first find the optimal pre- and post-filters as a function of the noise spectra $\Theta_+ = \{\Theta_+(e^{j\omega})\}_{\omega=-\pi}^{\pi}$ and $\Theta_- = \{\Theta_-(e^{j\omega})\}_{\omega=-\pi}^{\pi}$. Given these filters, we then find the side and central distortions (D_S, D_C) of the coder. We finally derive the mutual information rate within the system.

Let the side post-filter $G_s(e^{j\omega})$ and the central post-filter $G_c(e^{j\omega})$ be MMSE filters (i.e. Wiener filters) so that

$$G_s(e^{j\omega}) = \frac{F^*(e^{j\omega})S_X(e^{j\omega})}{|F(e^{j\omega})|^2 S_X(e^{j\omega}) + \Theta_+(e^{j\omega}) + \Theta_-(e^{j\omega})} \tag{52}$$

and

$$G_c(e^{j\omega}) = \frac{F^*(e^{j\omega})S_X(e^{j\omega})}{|F(e^{j\omega})|^2 S_X(e^{j\omega}) + \Theta_+(e^{j\omega})} \tag{53}$$

where $F(e^{j\omega})$ is the pre-filter. We match the pre-filter to the additive noise observed at the side decoders. Thus, we define

$$|F(e^{j\omega})|^2 \triangleq \frac{S_X(e^{j\omega}) - \Theta_+(e^{j\omega}) - \Theta_-(e^{j\omega})}{S_X(e^{j\omega})} \tag{54}$$

so that we have $G_s(e^{j\omega}) = F^*(e^{j\omega})$ which leads to

$$|F(e^{j\omega})|^2 = |G_s(e^{j\omega})|^2 = F(e^{j\omega})G_s(e^{j\omega}). \tag{55}$$

It is easy to see that the cross-product filter $G_c(e^{j\omega})F(e^{j\omega})$ satisfies

$$G_c(e^{j\omega})F(e^{j\omega}) = \frac{S_X(e^{j\omega}) - \Theta_+(e^{j\omega}) - \Theta_-(e^{j\omega})}{S_X(e^{j\omega}) - \Theta_-(e^{j\omega})} \tag{56}$$

and that

$$|G_c(e^{j\omega})|^2 = \frac{S_X(e^{j\omega})(S_X(e^{j\omega}) - \Theta_+(e^{j\omega}) - \Theta_-(e^{j\omega}))}{(S_X(e^{j\omega}) - \Theta_-(e^{j\omega}))^2}. \tag{57}$$

The side distortion D_S is given by

$$\begin{aligned} D_S &= \mathbb{E}[\bar{d}(\hat{X}_1, X)] && (58)\\ &= \mathbb{E}[(X(e^{j\omega})(F(e^{j\omega})G_s(e^{j\omega}) - 1)^2 + G_s(e^{j\omega})(Z_+(e^{j\omega}) + Z_-(e^{j\omega})))^2] && (59)\\ &= \frac{1}{2\pi}\int_{-\pi}^{\pi} \Theta_+(e^{j\omega}) + \Theta_-(e^{j\omega})\, d\omega && (60) \end{aligned}$$

and the central distortion D_C is given by

$$\begin{aligned} D_C &= \mathbb{E}[\bar{d}(\hat{X}_C, X)] && (61)\\ &= \mathbb{E}[(X(e^{j\omega})(F(e^{j\omega})G_c(e^{j\omega}) - 1)^2 + G_c(e^{j\omega})Z_+(e^{j\omega}))^2] && (62)\\ &= \frac{1}{2\pi}\int_{-\pi}^{\pi} \frac{S_X(e^{j\omega})\Theta_+(e^{j\omega})}{S_X(e^{j\omega}) - \Theta_-(e^{j\omega})}\, d\omega. && (63) \end{aligned}$$

At this point we recall that U is the pre-filtered version of X, i.e., $U(z) = F(z)X(z)$. Let $V_1 = U + N_1$ and $V_2 = U + N_2$ where $N_1 = Z_+ + Z_-$ and $N_2 = Z_+ - Z_-$ and note that $X, N_1,$ and N_2 are mutually independent. In [16], it was shown that the sum rate of a stationary source can be lower bounded by (with equality in the Gaussian case):

$$\begin{aligned} 2R &\geq \bar{I}(V_1, V_2; U) + \bar{I}(V_1; V_2) && (64)\\ &= \bar{h}(V_1) + \bar{h}(V_2) - \bar{h}(V_1, V_2|U), && (65) \end{aligned}$$

where for $i = 1, 2$,

$$\bar{h}(V_i) = \frac{1}{2}\log(2\pi e) + \frac{1}{4\pi}\int_{-\pi}^{\pi} \log(|F(e^{j\omega})|^2 S_X(e^{j\omega}) + \Theta_+(e^{j\omega}) + \Theta_-(e^{j\omega}))\, d\omega. \tag{66}$$

In fact, $\bar{h}(V_i) = \frac{1}{2}\log(P_e(V_i))$. Since $V_1, V_2,$ and U are jointly Gaussian, the conditional distribution of $(V_1, V_2)|U$ is also Gaussian. Let $\Phi_{N_1,N_2}(e^{j\omega}) = \Phi_{V_1,V_2|U}(e^{j\omega})$ denote the resulting

covariance matrix of the noises in a given frequency band $\omega \in [-\pi; \pi]$. It is easy to see that

$$\Phi_{N_1,N_2}(e^{j\omega}) = \begin{bmatrix} \Theta_+(e^{j\omega}) + \Theta_-(e^{j\omega}) & (\Theta_+(e^{j\omega}) + \Theta_-(e^{j\omega}))\rho(e^{j\omega}) \\ (\Theta_+(e^{j\omega}) + \Theta_-(e^{j\omega}))\rho(e^{j\omega}) & \Theta_+(e^{j\omega}) + \Theta_-(e^{j\omega}) \end{bmatrix}, \tag{67}$$

where the correlation coefficient $-1 < \rho(e^{j\omega}) \leq 1$ is given by [10]

$$\rho(e^{j\omega}) = \frac{\Theta_+(e^{j\omega}) - \Theta_-(e^{j\omega})}{\Theta_+(e^{j\omega}) + \Theta_-(e^{j\omega})}. \tag{68}$$

Let $|\cdot|$ denote the matrix determinant and notice that

$$|\Phi_{N_1,N_2}(e^{j\omega})| = (\Theta_+(e^{j\omega}) + \Theta_-(e^{j\omega}))^2(1 - \rho(e^{j\omega})^2) \tag{69}$$

$$= 4\Theta_+(e^{j\omega})\Theta_-(e^{j\omega}). \tag{70}$$

Since $\bar{h}(V_1, V_2|U) = \bar{h}(N_1, N_2)$, it follows by use of (65), (66) and (70) that the side description rate is given by

$$R = \frac{1}{4\pi}\int_{-\pi}^{\pi} \log\left(\frac{|F(e^{j\omega})|^2 S_X(e^{j\omega}) + \Theta_+(e^{j\omega}) + \Theta_-(e^{j\omega})}{2\sqrt{\Theta_+(e^{j\omega})\Theta_-(e^{j\omega})}}\right) d\omega \tag{71}$$

$$= \frac{1}{4\pi}\int_{-\pi}^{\pi} \log\left(\frac{S_X(e^{j\omega})}{2\sqrt{\Theta_+(e^{j\omega})\Theta_-(e^{j\omega})}}\right) d\omega. \tag{72}$$

This proves the theorem. ■

APPENDIX B
PROOF OF THEOREM 1

We recognize that the constrained optimization problem given by Corollary 1 forms an extended isoperimetric problem, which is a family of optimization problems well known in the literature on calculus of variations [7]. Using the cost functional (21), it is easy to show that the Lagrangian in this case is given by:

$$\mathcal{L}(\lambda_1, \lambda_2) = \frac{1}{4\pi}\log\left(\frac{S_X(e^{j\omega})}{2\sqrt{\Theta_+(e^{j\omega})\Theta_-(e^{j\omega})}}\right) + \frac{\lambda_1}{2\pi}(\Theta_+(e^{j\omega}) + \Theta_-(e^{j\omega})) + \frac{\lambda_2}{2\pi}\frac{S_X(e^{j\omega})\Theta_+(e^{j\omega})}{S_X(e^{j\omega}) - \Theta_-(e^{j\omega})}, \tag{73}$$

[10] If one is only interested in non-positive correlations, the following constraint is required: $\Theta_-(e^{j\omega}) \geq \Theta_+(e^{j\omega}) > 0, \forall\omega$.

where $\lambda_i \in \mathbb{R}, i = 1, 2$, are the scalar Lagrangian variables [7]. From (73) we obtain the following two differential equations:

$$\frac{\partial \mathcal{L}(\lambda_1, \lambda_2)}{\partial \Theta_+(e^{j\omega})} = -\frac{1}{8\pi}\frac{1}{\Theta_+(e^{j\omega})} + \frac{\lambda_1}{2\pi} + \frac{\lambda_2}{2\pi}\frac{S_X(e^{j\omega})}{S_X(e^{j\omega}) - \Theta_-(e^{j\omega})} \tag{74}$$

and

$$\frac{\partial \mathcal{L}(\lambda_1, \lambda_2)}{\partial \Theta_-(e^{j\omega})} = -\frac{1}{8\pi}\frac{1}{\Theta_-(e^{j\omega})} + \frac{\lambda_1}{2\pi} + \frac{\lambda_2}{2\pi}\frac{S_X(e^{j\omega})\Theta_+(e^{j\omega})}{(S_X(e^{j\omega}) - \Theta_-(e^{j\omega}))^2}. \tag{75}$$

Equating both (74) and (75) to zero and then solving for their joint solutions, yields

$$\Theta_-(e^{j\omega}) = \Psi^{\dagger}_{\lambda_1,\lambda_2}(e^{j\omega}) \tag{76}$$

and

$$\Theta_+(e^{j\omega}) = \frac{S_X(e^{j\omega}) - \Psi^{\dagger}_{\lambda_1,\lambda_2}(e^{j\omega})}{4S_X(e^{j\omega})(\lambda_1 + \lambda_2) - 4\lambda_1\Psi^{\dagger}_{\lambda_1,\lambda_2}(e^{j\omega})}, \tag{77}$$

which after elimating λ_2 simplifies to

$$\Theta_+(e^{j\omega}) = S_X(e^{j\omega}) - \Psi^{\dagger}_{\lambda_1,\lambda_2}(e^{j\omega}) + \frac{1}{2\lambda_1} - \frac{S_X(e^{j\omega})}{4\lambda_1\Psi^{\dagger}_{\lambda_1,\lambda_2}(e^{j\omega})}. \tag{78}$$

For a fixed pair $(\lambda_1, \lambda_2) \in \mathbb{R}^2$, $\Psi^{\dagger}_{\lambda_1,\lambda_2}(e^{j\omega})$ denotes a real (and positive) root of the third-order polynomial

$$\begin{aligned}\Psi^3(e^{j\omega}) &- \frac{4\lambda_1\lambda_2 S_X(e^{j\omega}) + 8\lambda_1^2 S_X(e^{j\omega}) + \lambda_1}{4\lambda_1^2}\Psi^2(e^{j\omega}) \\ &+ \frac{2\lambda_1 S_X(e^{j\omega}) + 2\lambda_2 S_X(e^{j\omega}) + 4\lambda_1\lambda_2 S_X^2(e^{j\omega}) + 4\lambda_1^2 S_X^2(e^{j\omega})}{4\lambda_1^2}\Psi(e^{j\omega}) - \frac{S_X^2(e^{j\omega})(\lambda_2 + \lambda_1)}{4\lambda_1^2}.\end{aligned} \tag{79}$$

Since (79) is a real third-order polynomial in $\Psi(e^{j\omega})$, three solutions are possible (of which two might be complex conjugates). Given a real polynomial $x^3(e^{j\omega}) + a_2(e^{j\omega})\, x^2(e^{j\omega}) + a_1(e^{j\omega})\, x(e^{j\omega}) + a_0(e^{j\omega})$, where the $a_i(e^{j\omega})$'s follows from (79), we let

$$\begin{aligned} p(e^{j\omega}) &= \frac{a_1(e^{j\omega})}{3} - \frac{a_2^2(e^{j\omega})}{9} \\ &= -\frac{1}{144\lambda_1^2}(-8\lambda_1 S_X(e^{j\omega}) - 16\lambda_2 S_X(e^{j\omega}) + 16\lambda_1\lambda_2 S_X^2(e^{j\omega}) + 16\lambda_1^2 S_X^2(e^{j\omega}) \\ &\quad + 16 S_X^2(e^{j\omega})\lambda_2^2 + 1)\end{aligned} \tag{80}$$

and

$$q(e^{j\omega}) = \frac{1}{6}(a_1(e^{j\omega})\, a_2(e^{j\omega}) - 3a_0(e^{j\omega})) - \frac{a_2^3(e^{j\omega})}{27} \tag{81}$$

$$= -\frac{1}{1728\lambda_1^3}\Big(96\lambda_1\lambda_2 S_X^2(e^{j\omega}) - 48\lambda_1^2 S_X^2(e^{j\omega}) - 64\lambda_2^3 S_X^3(e^{j\omega}) - 96\lambda_2^2 S_X^3(e^{j\omega})\lambda_1 + 96\lambda_2^2 S_X^2(e^{j\omega}) + 96\lambda_2 S_X^3(e^{j\omega})\lambda_1^2 + 24\lambda_2 S_X(e^{j\omega}) + 64\lambda_1^3 S_X^3(e^{j\omega}) + 12\lambda_1 S_X(e^{j\omega}) - 1\Big). \tag{82}$$

Moreover, let $s_1(e^{j\omega}) = \sqrt[3]{q(e^{j\omega}) + \sqrt{p(e^{j\omega})^3 + q(e^{j\omega})^2}}$ and $s_2(e^{j\omega}) = \sqrt[3]{q(e^{j\omega}) - \sqrt{p(e^{j\omega})^3 + q(e^{j\omega})^2}}$. Then, the three solutions are given by [19]

$$x_1(e^{j\omega}) = (s_1(e^{j\omega}) + s_2(e^{j\omega})) - \frac{a_2(e^{j\omega})}{3} \tag{83}$$

$$x_2(e^{j\omega}) = -\frac{1}{2}(s_1(e^{j\omega}) + s_2(e^{j\omega})) - \frac{a_2(e^{j\omega})}{3} + \frac{i\sqrt{3}}{2}(s_1(e^{j\omega}) - s_2(e^{j\omega})) \tag{84}$$

$$x_3(e^{j\omega}) = -\frac{1}{2}(s_1(e^{j\omega}) + s_2(e^{j\omega})) - \frac{a_2(e^{j\omega})}{3} - \frac{i\sqrt{3}}{2}(s_1(e^{j\omega}) - s_2(e^{j\omega})). \tag{85}$$

The discriminant $\Xi(e^{j\omega})$ of the third-order polynomial $x^3(e^{j\omega}) + a_2(e^{j\omega})\, x^2(e^{j\omega}) + a_1(e^{j\omega})\, x(e^{j\omega}) + a_0(e^{j\omega})$ is given by

$$\Xi(e^{j\omega}) = q^2(e^{j\omega}) + p^3(e^{j\omega}). \tag{86}$$

There are three cases to consider, depending upon the sign of $\Xi(e^{j\omega})$. If $\Xi(e^{j\omega}) > 0$, then there is one real root and two complex roots. If $\Xi(e^{j\omega}) < 0$, there are three real distinct roots. Finally, if $\Xi(e^{j\omega}) = 0$, there is a single real triple root (if $q(e^{j\omega}) = 0$) or one real root and one real double root (if $q(e^{j\omega}) \neq 0$) [19]. Thus, for every choice of (λ_1, λ_2), one may identify the admissible (i.e. the real and positive) solutions of (83)–(85).

A. Spectral Constraints

Recall that Θ_+ characterizes the noise spectrum of the central distortion and that the sum spectrum $\Theta_- + \Theta_+$ characterizes the noise spectrum of the side distortion. Thus, we require that $0 < \Theta_+(e^{j\omega}) < \Theta_-(e^{j\omega}) < S_X(e^{j\omega}), \Theta_-(e^{j\omega}) + \Theta_+(e^{j\omega}) \leq S_X(e^{j\omega})$, which further implies that $\Theta_+(e^{j\omega}) < S_X(e^{j\omega})/2, \forall \omega \in [-\pi; \pi]$. With this, we may use (76) and (78) and form the

inequality $\Theta_+(e^{j\omega}) + \Theta_-(e^{j\omega}) \leq S_X(e^{j\omega})$, which can be rewritten as

$$\Psi^{\dagger}_{\lambda_1,\lambda_2}(e^{j\omega}) \leq \frac{S_X(e^{j\omega})}{2}. \tag{87}$$

Moreover, considering the other direction of the inequality, i.e., $\Theta_+(e^{j\omega}) + \Theta_-(e^{j\omega}) > 0$, leads to

$$\Psi^{\dagger}_{\lambda_1,\lambda_2}(e^{j\omega}) > \frac{S_X(e^{j\omega})}{4\lambda_1 S_X(e^{j\omega}) + 2}. \tag{88}$$

It follows from (87) and (88) that $\lim_{\lambda_1 \to 0} \Psi^{\dagger}_{\lambda_1,\lambda_2}(e^{j\omega}) = S_X(e^{j\omega})/2$.

B. Zeros of Ξ

It easy to show that

$$\Xi(e^{j\omega}) = -\frac{S_X^4(e^{j\omega})(4\lambda_1^2 S_X^2(e^{j\omega}) + 1)}{432\lambda_1^6}(\lambda_2 - \xi_0^{\Xi}(e^{j\omega}))(\lambda_2 - \xi_1^{\Xi}(e^{j\omega}))(\lambda_2 - \xi_2^{\Xi}(e^{j\omega}))(\lambda_2 - \xi_3^{\Xi}(e^{j\omega})), \tag{89}$$

where $\{\xi_i^{\Xi}(e^{j\omega})\}$ are the four real roots of $\Xi(e^{j\omega})$ given by $\xi_0^{\Xi}(e^{j\omega}) = 0, \xi_1^{\Xi}(e^{j\omega}) = -\lambda_1$,

$$\xi_2^{\Xi}(e^{j\omega}) = -\frac{2S_X(e^{j\omega})\lambda_1 + 8S_X^3(e^{j\omega})\lambda_1^3 - 16S_X^2(e^{j\omega})\lambda_1^2 - 3 + 2\sqrt{2(2S_X^2(e^{j\omega})\lambda_1^2 + 1)^3}}{4S_X(e^{j\omega})(4S_X^2(e^{j\omega})\lambda_1^2 + 1)}, \tag{90}$$

$$\xi_3^{\Xi}(e^{j\omega}) = -\frac{2S_X(e^{j\omega})\lambda_1 + 8S_X^3(e^{j\omega})\lambda_1^3 - 16S_X^2(e^{j\omega})\lambda_1^2 - 3 - 2\sqrt{2(2S_X^2(e^{j\omega})\lambda_1^2 + 1)^3}}{4S_X(e^{j\omega})(4S_X^2(e^{j\omega})\lambda_1^2 + 1)}. \tag{91}$$

From the Kuhn-Tucker Theorem, it follows that the Lagrangian variables are non-negative, i.e. $\lambda_1, \lambda_2 \geq 0$, see [20] for details. Thus, we only have to consider non-negative multipliers and it follows that $\xi_1^{\Xi}(e^{j\omega}) \leq 0$. Clearly, $\xi_2^{\Xi}(e^{j\omega}) < \xi_3^{\Xi}(e^{j\omega}), \forall\omega$. Moreover, from Lemma 1 below, we notice that $\xi_3^{\Xi}(e^{j\omega}) > 0, \forall\lambda_1, \lambda_2 > 0$, but the sign of $\xi_2^{\Xi}(e^{j\omega})$ depends upon λ_1. If $\lambda_1 < 1/4S_X(e^{j\omega})$ then $\xi_2^{\Xi}(e^{j\omega}) < 0$, if $\lambda_1 = 1/4S_X(e^{j\omega})$ then $\xi_2^{\Xi}(e^{j\omega}) = 0$, and finally if $\lambda_1 > 1/4S_X(e^{j\omega})$ then $\xi_2^{\Xi}(e^{j\omega}) > 0$.

Lemma 1. *For* $\lambda_1 > 0, \xi_3^{\Xi}(e^{j\omega}) > 0$. *Moreover, the sign of* $\xi_2^{\Xi}(e^{j\omega})$ *(90) is given by:*

$$sign(\xi_2^{\Xi}(e^{j\omega})) = \begin{cases} - & \textit{if} \quad \lambda_1 > \frac{1}{4S_X(e^{j\omega})}, \\ 0 & \textit{if} \quad \lambda_1 = \frac{1}{4S_X(e^{j\omega})}, \\ + & \textit{if} \quad \lambda_1 < \frac{1}{4S_X(e^{j\omega})}. \end{cases} \tag{92}$$

Proof: We first show that $\xi_3^{\Xi}(e^{j\omega})$ (91) is non-negative. To do so, we show that

$$2S_X(e^{j\omega})\lambda_1 + 8S_X^3(e^{j\omega})\lambda_1^3 - 16S_X^2(e^{j\omega})\lambda_1^2 - 3 - 2\sqrt{2(2S_X^2(e^{j\omega})\lambda_1^2+1)^3} \leq 0, \qquad (93)$$

which means that (91) is non-negative. Let $\varphi_1(e^{j\omega}) = 2S_X(e^{j\omega})\lambda_1 + 8S_X^3(e^{j\omega})\lambda_1^3$ and $\varphi_2(e^{j\omega}) = 2\sqrt{2(2S_X^2(e^{j\omega})\lambda_1^2+1)^3}$ and notice that it is enough to show that $\varphi_1(e^{j\omega}) < \varphi_2(e^{j\omega}), \forall\omega$. Since $\varphi_1(e^{j\omega})$ and $\varphi_2(e^{j\omega})$ are both positive functions, we may work on their squares, i.e., $\varphi_1^2(e^{j\omega}) = 4S_X^2(e^{j\omega})\lambda_1^2 + 32S_X^4(e^{j\omega})\lambda_1^4 + 64S_X^6(e^{j\omega})\lambda_1^6$ and $\varphi_2^2(e^{j\omega}) = 64S_X^6(e^{j\omega})\lambda_1^6 + 192S_X^4(e^{j\omega})\lambda_1^4 + 192S_X^2(e^{j\omega})\lambda_1^2 + 64$. Forming the inequality $\varphi_2^2(e^{j\omega}) > \varphi_1^2(e^{j\omega})$ and collecting similar terms yields $64 > -188S_X^2(e^{j\omega})\lambda_1^2 - 160S_X^4(e^{j\omega})\lambda_1^4$ which is always satisfied for $\lambda_1 \in \mathbb{R}$. This proves the first part of the lemma.

We now consider the sign of $\xi_2^{\Xi}(e^{j\omega})$ (90). Let $\varphi_1 = 2x + 8x^3 - 16x^2 - 3$ and $\varphi_2 = 2\sqrt{2(2x^2+1)^3}$. The discriminant of φ_1 is strictly positive so φ_1 has only a single real root, which is located at $\xi = 1.96973$ where we note that $\xi > \frac{1}{4}$. Moreover, $x = 0 \Rightarrow \varphi_1 = -3$ and it follows that $\varphi_1 < 0$ for $x < \xi$ and $\varphi_1 > 0$ for $x > \xi$. Notice also that $\varphi_2 > 0$ for $x > 0$.

At this point we let $h = \varphi_1^2 - \varphi_2^2 = -256(z - \frac{i}{2})(z + \frac{i}{2})(z - \frac{1}{4})^3$, which is a fifth-order polynomial having a pair of complex conjugate roots at $x = \pm i/2$ and a real (triple) root at $x = 1/4$. Thus, h crosses the real line only once. Since $h = 1$ for $x = 0$ it follows that $h > 0$ for $x < 1/4$ and $h < 0$ for $x > 1/4$. Furthermore, $h = 0$ for $x = 1/4$.

Since $h > 0$ for $x < 1/4$ it follows that $\varphi_1^2 > \varphi_2^2$ which implies that $\varphi_1 + \varphi_2 < 0$ since $\varphi_1 < 0$ for $x < 1/4$. The first case of (92) now follows by inserting $x = \lambda_1 S_X(e^{j\omega})$ in φ_1 and remembering the additional sign from (91). Since $h = 0$ implies that $\varphi_1 + \varphi_2 = 0$, it immediately follows that $sign(\xi_2^{\Xi}(e^{j\omega})) = 0$ for $x = \lambda_1 S_X(e^{j\omega}) = 1/4$. Finally, for $h < 0$ we have $\varphi_2^2 > \varphi_1^2$ which implies that $\varphi_2 > \varphi_1$ since φ_2 is positive and it follows that $\xi_2^{\Xi}(e^{j\omega}) < 0$ for $\lambda_1 S_X(e^{j\omega}) > 1/4$. This proves the remaining parts of the lemma. ■

We have illustrated the possible zero locations of $\Xi(e^{j\omega})$ in Fig. 14 using the fact that $\lim_{\lambda_2 \to \pm\infty} \Xi(e^{j\omega}) = -\infty, \forall\omega$.

C. Negative Discriminant

In this case $\Xi(e^{j\omega}) = q^2(e^{j\omega}) + p^3(e^{j\omega}) < 0$ and we have three real solutions. It is easy to see that we must have $p(e^{j\omega}) < 0$ and $|p(e^{j\omega})|^3 > q^2(e^{j\omega})$. Let $z_1(e^{j\omega}) = q(e^{j\omega}) + \sqrt{\Xi(e^{j\omega})} = q(e^{j\omega}) + i\sqrt{-\Xi(e^{j\omega})}$ and $z_2(e^{j\omega}) = q(e^{j\omega}) - \sqrt{\Xi(e^{j\omega})} = q(e^{j\omega}) - i\sqrt{-\Xi(e^{j\omega})}$ and notice that

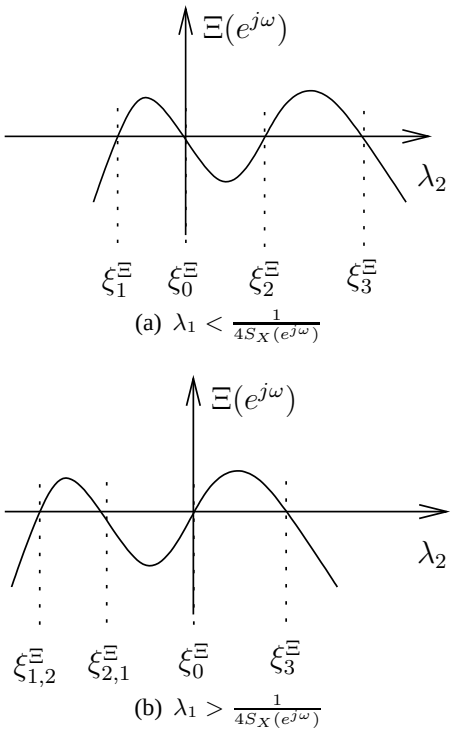

Fig. 14. The possible zero locations for the discriminant $\Xi(e^{j\omega})$ as a function of λ_2 for a given ω. We note that the ξ_i^{Ξ}'s are functions of ω.

$s_i(e^{j\omega}) = \sqrt[3]{z_i(e^{j\omega})}, i = 1, 2$. Since $\Xi(e^{j\omega}), p(e^{j\omega}) < 0$, it follows that $|z_1(e^{j\omega})| = |z_2(e^{j\omega})| = \sqrt{-p(e^{j\omega})^3} = \sqrt{|p(e^{j\omega})|^3}$. Moreover, the phase is given by

$$\phi_1(e^{j\omega}) = \begin{cases} \arctan(\sqrt{-\Xi(e^{j\omega})}/q(e^{j\omega})), & q(e^{j\omega}) > 0, \\ \pi + \arctan(\sqrt{-\Xi(e^{j\omega})}/q(e^{j\omega})), & q(e^{j\omega}) < 0, \\ \pi/2, & q(e^{j\omega}) = 0, \end{cases} \tag{94}$$

and $\phi_2(e^{j\omega}) = -\phi_1(e^{j\omega})$. Thus, $\phi_1(e^{j\omega}) \in [0; \pi]$. The value of $\phi_1(e^{j\omega})$ depends upon $q(e^{j\omega})$, which is a third-order real polynomial in λ_2 having a negative (or zero) discriminant. Thus, it has three real roots $\{\xi_i^q(e^{j\omega})\}, i = 0, 1, 2,$ which after some algebra can be shown to be given by

$$\xi_0^q(e^{j\omega}) = \frac{1}{2S_X(e^{j\omega})}\sqrt{6}\sqrt{2S_X^2(e^{j\omega})\lambda_1^2 + 1}\cos\left(\frac{\phi_q(e^{j\omega})}{3}\right) - \frac{\lambda_1}{2} + \frac{1}{2S_X(e^{j\omega})}, \tag{95}$$

$$\xi_1^q(e^{j\omega}) = -\frac{1}{4S_X(e^{j\omega})}\sqrt{6}\sqrt{2S_X^2(e^{j\omega})\lambda_1^2+1}\left(\sqrt{3}\sin\left(\frac{\phi_q(e^{j\omega})}{3}\right)+\cos\left(\frac{\phi_q(e^{j\omega})}{3}\right)\right)-\frac{\lambda_1}{2} + \frac{1}{2S_X(e^{j\omega})}, \tag{96}$$

$$\xi_2^q(e^{j\omega}) = \frac{1}{4S_X(e^{j\omega})}\sqrt{6}\sqrt{2S_X^2(e^{j\omega})\lambda_1^2+1}\left(-\sqrt{3}\sin\left(\frac{\phi_q(e^{j\omega})}{3}\right)+\cos\left(\frac{\phi_q(e^{j\omega})}{3}\right)\right)-\frac{\lambda_1}{2} + \frac{1}{2S_X(e^{j\omega})}, \tag{97}$$

where

$$\phi_q(e^{j\omega}) = \arctan\left(\frac{1}{9}\sqrt{768S_X^6(e^{j\omega})\lambda_1^6+1152S_X^4(e^{j\omega})\lambda_1^4+576S_X^2(e^{j\omega})\lambda_1^2+15}\right). \tag{98}$$

Moreover, $\lim_{\lambda_2\to\infty} q(e^{j\omega}) = \infty$ and $\lim_{\lambda_2\to-\infty} q(e^{j\omega}) = -\infty$. Thus, $q(e^{j\omega}) > 0$ if $\lambda_2 > \xi_0^q(e^{j\omega})$ or if $\xi_1^q(e^{j\omega}) < \lambda_2 < \xi_2^q(e^{j\omega})$.

With this, it is easy to show that the solutions (roots), $\{x_i(e^{j\omega})\}_{i=1}^3$, as given by (83)–(85), can be written as

$$x_1(e^{j\omega}) = 2\sqrt{|p(e^{j\omega})|}\cos(\phi_1(e^{j\omega})/3) - \frac{a_2(e^{j\omega})}{3}, \tag{99}$$

$$x_2(e^{j\omega}) = -\sqrt{|p(e^{j\omega})|}\Big(\cos(\phi_1(e^{j\omega})/3) + \sqrt{3}\sin(\phi_1(e^{j\omega})/3)\Big) - \frac{a_2(e^{j\omega})}{3}, \tag{100}$$

$$x_3(e^{j\omega}) = -\sqrt{|p(e^{j\omega})|}\Big(\cos(\phi_1(e^{j\omega})/3) - \sqrt{3}\sin(\phi_1(e^{j\omega})/3)\Big) - \frac{a_2(e^{j\omega})}{3}. \tag{101}$$

We note that

$$\min_{\zeta\in[0;\pi]} 2\cos(\zeta/3) \geq \max_{\zeta\in[0;\pi]} -(\cos(\zeta/3) - \sqrt{3}\sin(\zeta/3)) \tag{102}$$

and that

$$\min_{\zeta\in[0;\pi]} -(\cos(\zeta/3) - \sqrt{3}\sin(\zeta/3)) \geq \max_{\zeta\in[0;\pi]} -(\cos(\zeta/3) + \sqrt{3}\sin(\zeta/3), \tag{103}$$

which implies that $x_1(e^{j\omega}) \geq x_3(e^{j\omega}) \geq x_2(e^{j\omega})$ for any pair (λ_1, λ_2) and for all $\omega \in [-\pi; \pi]$.

Let us first consider the solution $x_3(e^{j\omega})$ given by (101). From Lemma 2 below, it follows that $x_3(e^{j\omega}) > S_X(e^{j\omega})/2$, which violates the spectral constraint (87). Moreover, since $x_1(e^{j\omega}) > x_3(e^{j\omega})$, we deduce that $x_2(e^{j\omega})$ given by (100) is the only admissible solution.

Lemma 2. *Let $\Xi(e^{j\omega}) < 0$. Then, for any positive λ_1 and $\lambda_2, x_3(e^{j\omega}) > S_X(e^{j\omega})/2, \forall\omega$, where $x_3(e^{j\omega})$ is given by (101).*

Proof: Since $\Xi(e^{j\omega}) < 0$, we only need to consider $p(e^{j\omega}) < 0$. Thus, $\sqrt{|p(e^{j\omega})|} = \sqrt{-p(e^{j\omega})}$. Moreover, $\frac{\partial^2}{\partial\lambda_2^2}\sqrt{|p(e^{j\omega})|} = \frac{c(e^{j\omega})\,(4S_X^2(e^{j\omega})\lambda_1^2-1)}{\sqrt{|p(e^{j\omega})|^3}}$, for some everywhere positive function $c(e^{j\omega})$. It follows that for $\lambda_1 > \frac{1}{2S_X(e^{j\omega})}$, $\sqrt{|p(e^{j\omega})|}$ has increasing slope in λ_2. Taking the limit $\lambda_2 \to \infty$ shows that the maximum slope of $\sqrt{|p(e^{j\omega})|}$ is $\frac{S_X(e^{j\omega})}{3\lambda_1}$. On the other hand, $-\frac{a_2(e^{j\omega})}{3} > 3S_X(e^{j\omega})/2$ and is increasing in λ_2 with constant slope $\frac{S_X(e^{j\omega})}{3\lambda_1}$. Moreover, $\cos(\phi_1(e^{j\omega})/3) - \sqrt{3}\sin(\phi_1(e^{j\omega})/3) \leq 1$. Thus, $x_3(e^{j\omega}) \geq -\sqrt{|p(e^{j\omega})|} - \frac{a_2(e^{j\omega})}{3} > 3S_X(e^{j\omega})/2$ for $\lambda_1 > 1/(2S_X(e^{j\omega}))$.

Let us now instead assume that $\lambda_1 < \frac{1}{2S_X(e^{j\omega})}$, which is a high distortion situation since from (88) it follows that having $\lambda_1 < 1/(2S_X(e^{j\omega}))$ implies that $\Theta_-(e^{j\omega}) > S_X(e^{j\omega})/4, \forall\lambda_2$. In this case $-\sqrt{|p(e^{j\omega})|} - a_2(e^{j\omega})/3$ is concave in λ_2. Clearly, $[-\sqrt{|p(e^{j\omega})|} - a_2/3]_{\lambda_2=0} > S_X(e^{j\omega})/2$ and we know from above that in the limit $\lambda_2 \to \infty, -\sqrt{|p(e^{j\omega})|} - a_2(e^{j\omega})/3 > S_X(e^{j\omega})/2$. Thus, since we can lower bound a concave function by an affine function, it follows that $-\sqrt{|p(e^{j\omega})|} - a_2(e^{j\omega})/3 > S_X(e^{j\omega})/2$. Thus, $x_3(e^{j\omega}) > S_X(e^{j\omega})/2$ as was to be proven. ■

D. Positive Discriminant

In this case $\Xi(e^{j\omega}) > 0$ and we have only a single real solution given by $x_1(e^{j\omega})$ (83).

E. Zero Discriminant

In this case $\Xi(e^{j\omega}) = 0$, which is possible if $-p^3(e^{j\omega}) = q^2(e^{j\omega})$. The positive zeros of $\Xi(e^{j\omega})$ are given by $\xi_2^{\Xi}(e^{j\omega}), \xi_3^{\Xi}(e^{j\omega})$, where the former is only positive if $\lambda_1 < \frac{1}{4S_X(e^{j\omega})}$. Since $q(e^{j\omega}) \neq 0$ when $\Xi(e^{j\omega}) = 0$, there are two real solutions i.e., $x_1(e^{j\omega})$ and $x_2(e^{j\omega}) = x_3(e^{j\omega})$. We now show that $x_1(e^{j\omega})$ is the desired solution.

Let $\lambda_2 = \xi_3^{\Xi}(e^{j\omega})$ for some ω. Then it is easy to show that $s_1(e^{j\omega}) = s_2(e^{j\omega}) < 0$ and clearly $-a_2(e^{j\omega})/3 > S_X(e^{j\omega})/2$. Thus, $x_2(e^{j\omega}) = x_3(e^{j\omega}) = -\frac{1}{2}(s_1(e^{j\omega}) + s_2(e^{j\omega})) - a_2(e^{j\omega})/3 > S_X(e^{j\omega})/2$, which is not an admissible solution.

Now let $\lambda_2 = \xi_2^{\Xi}(e^{j\omega})$, which is positive if and only if $0 < \lambda_1 < 1/(4S_X(e^{j\omega}))$. Moreover, assume that $q(e^{j\omega}) < 0$ since otherwise $x_2(e^{j\omega}) = x_3(e^{j\omega})$ is clearly greater than $S_X(e^{j\omega})/2$. We

first show that $p(e^{j\omega}) < 0$ for $\lambda_2 = \xi_2^{\Xi}(e^{j\omega})$. After some algebra, we get

$$p(e^{j\omega})|_{\lambda_2=\xi_2^{\Xi}(e^{j\omega})} = \frac{1}{72\lambda_1^2(4S_X^2(e^{j\omega})\lambda_1^2+1)^2}(\varphi_1(e^{j\omega}) - \varphi_2(e^{j\omega})), \tag{104}$$

where

$$\varphi_1(e^{j\omega}) = 16\sqrt{2}\sqrt{(2S_X^2(e^{j\omega})\lambda_1^2+1)^3}S_X^2(e^{j\omega})\lambda_1^2 + 2\sqrt{2}\sqrt{(2S_X^2(e^{j\omega})\lambda_1^2+1)^3} \tag{105}$$

and

$$\varphi_2(e^{j\omega}) = 3 + 26S_X^2(e^{j\omega})\lambda_1^2 + 104\lambda_1^4 S_X^4(e^{j\omega}) + 128S_X^6(e^{j\omega})\lambda_1^6. \tag{106}$$

Since $\varphi_1(e^{j\omega})$ and $\varphi_2(e^{j\omega})$ are both positive functions, we can work on their squares, and form the inequality $\varphi_2^2(e^{j\omega}) - \varphi_1^2(e^{j\omega})$, that is

$$\begin{aligned}\varphi_2^2(e^{j\omega}) - \varphi_1^2(e^{j\omega}) = 1 - 20S_X^2(e^{j\omega})\lambda_1^2 - 76\lambda_1^4 S_X^4(e^{j\omega}) + 1504S_X^6(e^{j\omega})\lambda_1^6 + 10304S_X^8(e^{j\omega})\lambda_1^8 \\ + 22528\lambda_1^{10}S_X^{10}(e^{j\omega}) + 16384S_X^{12}(e^{j\omega})\lambda_1^{12},\end{aligned} \tag{107}$$

which is clearly positive for all $0 < \lambda_1 \leq 1/(4S_X(e^{j\omega}))$.

Let us now consider the zeros of $\Xi(e^{j\omega}) = q^2(e^{j\omega}) + p^3(e^{j\omega})$ and $q^2(e^{j\omega})$ from a geometric point of view. First, $q(e^{j\omega})$ is a third-order polynomial and $q^2(e^{j\omega})$ is a non-negative sixth-order polynomial that shares zeros with $q(e^{j\omega})$. Moreover, $p(e^{j\omega}) < 0$ as we established above and therefore $p^3(e^{j\omega}) < 0$ for $\lambda_2 = \xi_2^{\Xi}(e^{j\omega})$. If we consider the middle zero of $q^2(e^{j\omega})$, i.e., $\xi_2^q(e^{j\omega})$, then adding the negative function $p^3(e^{j\omega})$ to $q^2(e^{j\omega})$ will result in two zeros around the point $\lambda_2 = \xi_2^q(e^{j\omega})$ instead of a single zero at $\lambda_2 = \xi_2^q(e^{j\omega})$. In fact, the smaller of the zeros becomes $\xi_1^{\Xi}(e^{j\omega})$ and the larger zero becomes $\xi_2^{\Xi}(e^{j\omega})$. But then clearly $\xi_0^q(e^{j\omega}) > \xi_2^{\Xi}(e^{j\omega}) \geq \xi_2^q(e^{j\omega})$ and it follows that $q(e^{j\omega}) < 0$ for $\lambda_2 = \xi_2^{\Xi}(e^{j\omega})$. This shows that $x_2(e^{j\omega}) = x_3(e^{j\omega}) > S_X(e^{j\omega})/2$ also for $\lambda_2 = \xi_2^{\Xi}(e^{j\omega})$.

The solution for $\Xi(e^{j\omega}) = 0$, is therefore given by $x_1(e^{j\omega})$.

F. Summarizing Solutions

In the above we have shown that there is always only a single possible solution for any λ_1, λ_2. Specifically, if $\Xi(e^{j\omega}) < 0$, then the optimal solution is $x_2(e^{j\omega})$ (100) whereas if $\Xi(e^{j\omega}) \geq 0$, then the optimal solution is $x_1(e^{j\omega})$ (84). In all cases, the spectral constraints in Appendix B-A must be satisfied.

This proves the theorem. ■

APPENDIX C
PROOF OF PROPOSITION 5.

A. Case $\lambda_1 > 0$ and $\lambda_2 \gg 1$

In this case, we note that

$$\Xi(e^{j\omega}) = -\frac{\lambda_2^4 S_X^4(e^{j\omega})}{432\lambda_1^6}(1 + 4S_X^2(e^{j\omega})\lambda_1^2) + \mathcal{O}\Big(\frac{\lambda_2^3}{\lambda_1^3}\Big). \tag{108}$$

It follows that $\Xi(e^{j\omega}) < 0$ for large λ_2. Furthermore,

$$q(e^{j\omega}) = \frac{\lambda_2^3 S_X^3(e^{j\omega})}{27\lambda_1^3} + \mathcal{O}\Big(\frac{\lambda_2^2}{\lambda_1^2}\Big) \tag{109}$$

and $\phi_1(e^{j\omega}) = \arctan\left(\frac{\sqrt{-\Xi(e^{j\omega})}}{q(e^{j\omega})}\right)$.

We use the solution $x_2(e^{j\omega})$ given by (84) and need to carefully address its limiting behavior in λ_2, since the dominating terms cancel. The first-order Taylor approximation of $\arctan(x)$ is $\arctan(x) = x + \mathcal{O}(x^2), \forall |x| \leq 1$. Thus,

$$\phi_1(e^{j\omega}) = \arctan\left(\frac{\sqrt{-\Xi(e^{j\omega})}}{q(e^{j\omega})}\right) = \frac{3\sqrt{3}}{4S_X(e^{j\omega})\lambda_2}\sqrt{1 + 4S_X^2(e^{j\omega})\lambda_1^2} + \mathcal{O}\left(\frac{\lambda_1^3}{\sqrt{\lambda_2^3}}\right), \tag{110}$$

where the approximation becomes an equality in the limit as $\lambda_2 \to \infty$ since this implies that $\phi_1(e^{j\omega}) \to 0$. Similarly, for all x,

$$\cos(x/3) + \sqrt{3}\sin(x/3) = 1 + \frac{\sqrt{3}}{3}x + \mathcal{O}(x^2), \quad (\cos(x/3) + \sqrt{3}\sin(x/3))^2 = 1 + \frac{2\sqrt{3}}{3}x + \mathcal{O}(x^2). \tag{111}$$

Let $\alpha(e^{j\omega}) = \cos(\phi_1(e^{j\omega})/3) + \sqrt{3}\sin(\phi_1(e^{j\omega})/3)$. Then, we can write

$$x_2(e^{j\omega}) = -\sqrt{|p(e^{j\omega})|}\alpha(e^{j\omega}) - \frac{a_2(e^{j\omega})}{3} \tag{112}$$

$$= \frac{|p(e^{j\omega})|\alpha(e^{j\omega})^2 - \frac{a_2(e^{j\omega})^2}{9}}{-\sqrt{|p(e^{j\omega})|}\alpha(e^{j\omega}) + \frac{a_2(e^{j\omega})}{3}}. \tag{113}$$

From (111) and using (110), it follows that

$$\alpha(e^{j\omega})^2 = 1 + \frac{3}{2S_X(e^{j\omega})\lambda_2}\sqrt{1 + 4S_X^2(e^{j\omega})\lambda_1^2} + \mathcal{O}\left(\frac{\lambda_1^3}{\sqrt{\lambda_2^3}}\right). \tag{114}$$

With this, we can write the numerator of (113) as

$$|p(e^{j\omega})|\alpha(e^{j\omega})^2 - \frac{a_2(e^{j\omega})^2}{9} = -\frac{S_X(e^{j\omega})\lambda_2}{6\lambda_1^2}\Big(2S_X(e^{j\omega})\lambda_1 + 1 - \sqrt{1+4S_X^2(e^{j\omega})\lambda_1^2}\Big) + \mathcal{O}\Big(\frac{\lambda_1}{\sqrt{\lambda_2}}\Big). \tag{115}$$

On the other hand, since $\lim_{\lambda_2\to\infty}\alpha(e^{j\omega}) = 1, \forall\omega$, the denominator of (113) can be written as (for large λ_2)

$$-\sqrt{|p(e^{j\omega})|}\alpha(e^{j\omega}) + \frac{a_2(e^{j\omega})}{3} \approx -\frac{2S_X(e^{j\omega})\lambda_2}{3\lambda_1}. \tag{116}$$

Substituting (115) and (116) into (113) yields

$$\Theta_-(e^{j\omega}) = \frac{1}{4\lambda_1}\Big(2S_X(e^{j\omega})\lambda_1 + 1 - \sqrt{1+4S_X^2(e^{j\omega})\lambda_1^2}\Big) + \mathcal{O}\left(\frac{\lambda_1^2}{\sqrt{\lambda_2^3}}\right), \tag{117}$$

so that

$$\lim_{\lambda_2\to\infty}\Theta_-(e^{j\omega}) = \lim_{\lambda_2\to\infty}x_2(e^{j\omega}) = \frac{1}{4\lambda_1}\Big(2S_X(e^{j\omega})\lambda_1 + 1 - \sqrt{1+4S_X^2(e^{j\omega})\lambda_1^2}\Big). \tag{118}$$

B. Case $\lambda_1, \lambda_2 \gg 1$

We note that when assuming $\lambda_1/\sqrt[3]{\lambda_2} \to 0$, then the results for finite λ_1 in Section C-A remain valid. We rewrite (117) as

$$\Theta_-(e^{j\omega}) = \frac{1}{4\lambda_1}\Big(2S_X(e^{j\omega})\lambda_1 + 1 - \sqrt{1+4S_X^2(e^{j\omega})\lambda_1^2}\Big)\frac{-(2S_X(e^{j\omega})\lambda_1+1) - \sqrt{1+4S_X^2(e^{j\omega})\lambda_1^2}}{-(2S_X(e^{j\omega})\lambda_1+1) - \sqrt{1+4S_X^2(e^{j\omega})\lambda_1^2}} + \mathcal{O}\left(\frac{\lambda_1^2}{\sqrt{\lambda_2^3}}\right) \tag{119}$$

$$= \frac{1}{4\lambda_1}\frac{4S_X(e^{j\omega})\lambda_1}{\sqrt{1+4S_X^2(e^{j\omega})\lambda_1^2} + 2S_X(e^{j\omega})\lambda_1 + 1} + \mathcal{O}\left(\frac{\lambda_1^2}{\sqrt{\lambda_2^3}}\right) \tag{120}$$

$$= \frac{1}{4\lambda_1}c_{\lambda_1}(e^{j\omega}) + \mathcal{O}\left(\frac{\lambda_1^2}{\sqrt{\lambda_2^3}}\right), \tag{121}$$

where $c_{\lambda_1}(e^{j\omega}) = \mathcal{O}(1)$ and $\lim_{\lambda_1\to\infty}c_{\lambda_1}(e^{j\omega}) = 1, \forall\omega$. Inserting this into (27) yields

$$\Theta_+(e^{j\omega}) = \frac{1}{4(\lambda_1+\lambda_2) + \mathcal{O}\left(\frac{\lambda_1^2}{\sqrt{\lambda_2^3}}\right)} + \mathcal{O}\left(\frac{\lambda_1^2}{\lambda_1\sqrt{\lambda_2^3}+\lambda_2\sqrt{\lambda_2^3}} + \frac{1}{\lambda_1^2+\lambda_1\lambda_2}\right). \tag{122}$$

Finally, it follows from (121) and (122) that

$$\lim_{\substack{\lambda_1,\lambda_2\to\infty \\ \lambda_1/\sqrt[3]{\lambda_2}\to 0}} \lambda_1\Theta_- = \frac{1}{4}, \tag{123}$$

and

$$\lim_{\substack{\lambda_1,\lambda_2\to\infty \\ \lambda_1/\sqrt[3]{\lambda_2}\to 0}} \lambda_1\Theta_+(\lambda_1+\lambda_2) = \frac{1}{4}. \tag{124}$$

■

REFERENCES

[1] L. Ozarow, "On a source-coding problem with two channels and three receivers," *Bell System Technical Journal*, vol. 59, pp. 1909 – 1921, December 1980.

[2] J. Chen, C. Tian, and S. Diggavi, "Multiple description coding for stationary Gaussian sources," *IEEE Trans. Inf. Theory*, vol. 55, no. 6, pp. 2868–2881, June 2009.

[3] J. Østergaard and R. Zamir, "Multiple-description coding by dithered delta-sigma quantization," *IEEE Trans. Inf. Theory*, vol. 55, no. 10, pp. 4661–4675, October 2009.

[4] R. Zamir, "Shannon type bounds for multiple descriptions of a stationary source," *Journal of Combinatorics, Information and System Sciences*, pp. 1 – 15, December 2000.

[5] J. Chen, C. Tian, T. Berger, and S. S. Hemami, "Multiple description quantization via Gram-Schmidt orthogonalization," *IEEE Trans. Inf. Theory*, vol. 52, no. 12, pp. 5197 – 5217, December 2006.

[6] A. Kolmogorov, "On the Shannon theory of information transmission in the case of continuous signals," *IRE Trans. Inf. Theory.*, vol. IT-2, pp. 102–108, 1956.

[7] R. Weinstock, *Variational calculus*. Dover Publications, 1974.

[8] R. Zamir, Y. Kochman, and U. Erez, "Achieving the Gaussian rate-distortion function by prediction," *IEEE Trans. Inf. Theory*, vol. 54, no. 7, pp. 3354–3364, July 2008.

[9] A. Ingle and V. A. Vaishampayan, "DPCM system design for diversity systems with applications to packetized speech," *IEEE Trans. Speech and Audio Proc.*, vol. 3, no. 1, January 1995.

[10] S. L. Regunathan and K. Rose, "Efficient prediction in multiple description video coding," in *Proc. Int. Conf. on Image Proc.*, vol. 1, 2000, pp. 1020 – 1023.

[11] V. A. Vaishampayan and S. John, "Balanced interframe multiple description video compression," in *Proc. Int. Conf. on Image Proc.*, vol. 3, 1999, pp. 812 – 816.

[12] R. Nathan and R. Zamir, "Multiple description video coding with un-quantized prediction loop," in *Proc. Int. Conf. on Image Proc.*, vol. 1, 2001, pp. 982 – 985.

[13] H. L. Van Trees, *Detection, estimation, and modulation theory*. Wiley, NY, 1968.

[14] R. Zamir and M. Feder, "Information rates of pre/post filtered dithered quantizers," *IEEE Trans. Info. Theory*, vol. 42, no. 5, pp. 1340 – 1353, September 1996.

[15] ——, "On lattice quantization noise," *IEEE Trans. Info. Theory*, vol. 42, no. 4, pp. 1152 – 1159, July 1996.

[16] R. Zamir, "Gaussian codes and shannon bounds for multiple descriptions," *IEEE Trans. Inf. Theory*, vol. 45, no. 7, pp. 2629 – 2636, November 1999.

[17] R. G. Gallager, *Information theory and reliable communication*. Wiley, NY, 1968.

[18] N. S. Jayant and P. Noll, *Digital coding of waveforms*. Englewoods Cliffs, NJ: Prentice-Hall, 1984.

[19] M. Abramovitz and I. A. Stegun, Eds., *Handbook of mathematical functions*, 9th ed. Dover Publications, 1973.

[20] D. G. Luenberger, *Optimization by vector space methods*. John Wiley and Sons, 1969.